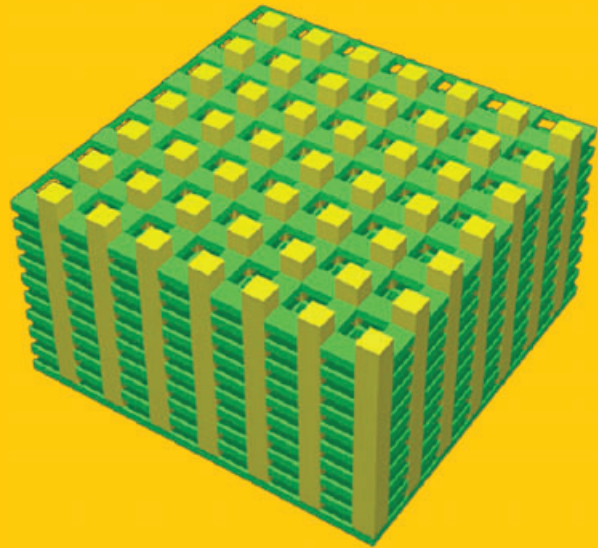


**Abstract** Nature began developing photonic nanoarchitectures millions of years before humankind. Often, in the living world, color is a communication channel that may influence the chance of the individual surviving as well as the chance to reproduce. Therefore, natural color-generating structures are highly optimized by many millennia of evolution. In this review, a survey is presented of the development of natural photonic crystal-type nanoarchitectures occurring in butterflies and beetles from the standpoint of physics and materials science, covering the past ten years. One-, two-, and three-dimensional structures are reviewed, emphasizing the role that disorder, or irregularity, may play in natural nanoarchitectures to achieve certain visual effects. The characterization, modeling methods, and rapidly growing number of bioinspired or biomimetic applications are discussed.



## Photonic nanoarchitectures in butterflies and beetles: valuable sources for bioinspiration

László Péter Biró<sup>1,\*</sup> and Jean-Pol Vigneron<sup>2</sup>

### 1. Introduction and brief overview

Photonic crystals (PhCs), or photonic band gap (PBG) materials, introduced to the physics and materials science communities only twenty years ago by Yablonovitch [1] and John [2], have been present in the living world for millions of years. The occurrence of PBG materials extends from animals living deep in the sea [3] to butterflies and birds flying high in the sky [4]. For a long time, studies focusing on these photonic nanoarchitectures were regarded as exotic and primarily for biologists with an affinity for physics, or quite early on, for prestigious scientists in optics, interested in light propagation and color, like Hooke [5], Newton [6], and Rayleigh [7].

The vigorous development of nanoscience and nanotechnology, together with the fast convergence of physics and materials science with biology, has renewed interest in naturally occurring photonic nanoarchitectures (Fig. 1). The motivation of industry is to be able to manufacture products with attractive aesthetics and convenient properties [8]. The benefit of basic science is the extraction of new bioinspired construction principles for the production of manmade PhCs and PBG materials.

An organism's visual aspect, or optical communication, has played a very important role in the evolution of most

of day-living animals [9]. Animals use their colors for sexual communication [10–12], for cryptic behavior [13–16], and for warning predators [17]. Color is subjected to strong evolutionary pressure, leading to the development of highly sophisticated photonic nanoarchitectures. Sometimes these nanoarchitectures may combine various types of PBG materials with fluorescence [18] and microfluidics [19] to achieve the desired optical effects. For example, the Panamanian tortoise beetle (*Charidotella egregia*) [19], when disturbed, can change color from shiny golden to mat red in a matter of minutes (Fig. 2). Clever ways may be found to emit highly directional signals [18]. These photonic natural nanoarchitectures constitute an invaluable library of 'blueprints'.

The extensive research effort into photonic nanoarchitectures of biological origin that has taken place over recent years (Fig. 1) has largely been motivated by their potential in a diverse array of applications. These applications include the direct use of the biologically evolved nanoarchitectures [20, 21] as templates for producing artificial photonic nanostructures [22–24] or mixed natural-artificial systems [23, 25], and the extraction of the basic construction principles from biological examples in order to design new types of bioinspired artificial structures [26–30]. As an example, work is currently underway for using the cells making up the scales of *Morpho* butterflies in order to achieve

<sup>1</sup> Research Institute for Technical Physics and Materials Science, POB 49, 1525 Budapest, Hungary <sup>2</sup> Facultés Universitaires Notre-Dame de la Paix, Rue de Bruxelles 61, 5000 Namur, Belgium

\* Corresponding author: e-mail: biro@mfa.kfki.hu, Phone: +36 1 3922681, Fax: +36 1 3922226

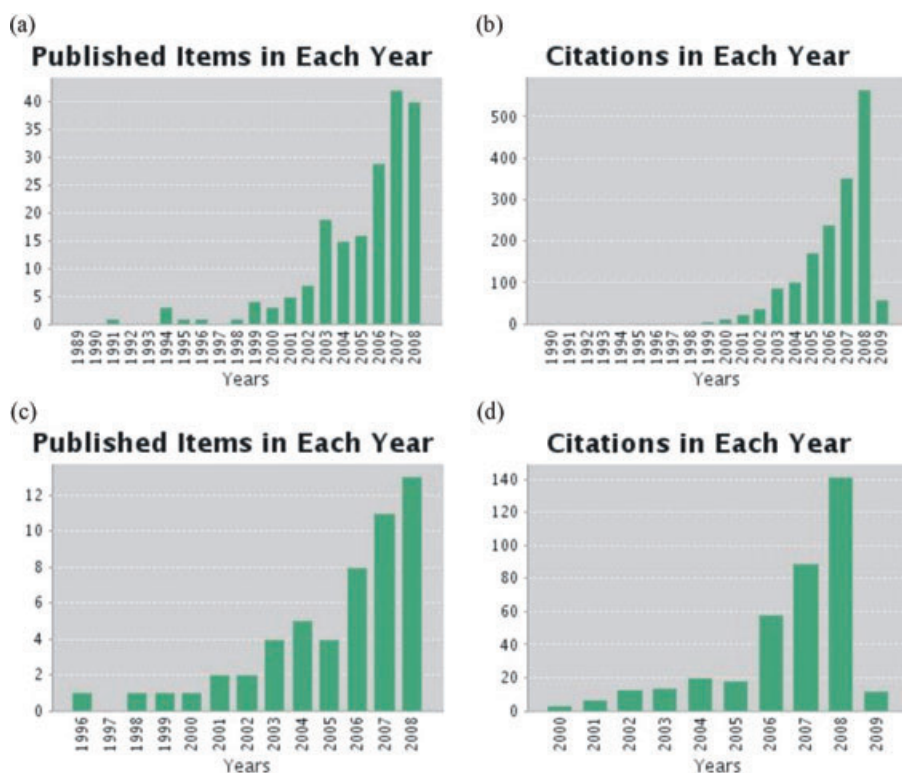


**Figure 1** (online color at: [www.lpr-journal.org](http://www.lpr-journal.org)) a) Number of published papers in the field of structural color of biological origin, and b) number of citations in each year of papers dealing with this topic. c) Selection of papers restricted to structural colors in butterflies and beetles, and d) number of citations of these paper in each year. (Source: search in the Web of Science database as of 6 February 2009.)

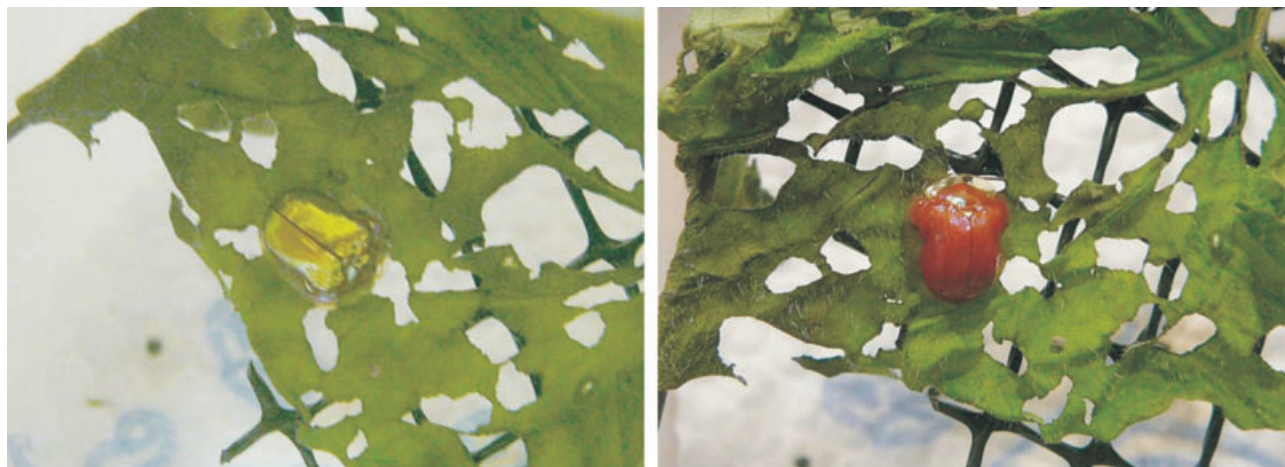


**Figure 2** (online color at: [www.lpr-journal.org](http://www.lpr-journal.org)) The Panamanian tortoise beetle before disturbance (left) and after disturbance (right). The two images are separated in time by a few minutes. The color change is fully reversible.

the production of the scales *in vitro* [31]. A very different approach to produce artificial *Morpho*-like colors is based on a substrate, with the carefully chosen combination of regular and random structures at the nanometer scale [32].

At this point, it is useful to clarify the difference between biomimetic and bioinspired approaches. Biomimetic approaches tend to reproduce the natural structure with the highest possible degree of fidelity, while bioinspired approaches extract new principles from structures found in the living world and implement those using different materials and different structural solutions [26, 27, 32].

Extensive studies have been published on butterfly wing coloration, which is frequently attributable to pigments [33],

a topic not discussed in this review. Ghiradella carried out pioneering work in the field of structural colors of butterflies [34–38]. A butterfly wing is a flat, double plate of cuticle covered by a dense tapestry of scales with rough dimensions of approximately 50–100  $\mu\text{m}$  by 15–50  $\mu\text{m}$  [36]. There are typically two layers of scales: larger cover scales and smaller ground scales arranged alternately in rows. The cover scales are architecturally more specialized and, with some exceptions, are generally responsible for the wing color [36]. The scales are primarily composed of chitin and have a shape of an elongated and flattened sack. Photonic nanoarchitectures may occupy the volume of this sack, or they may exist as a part of various structural elements such

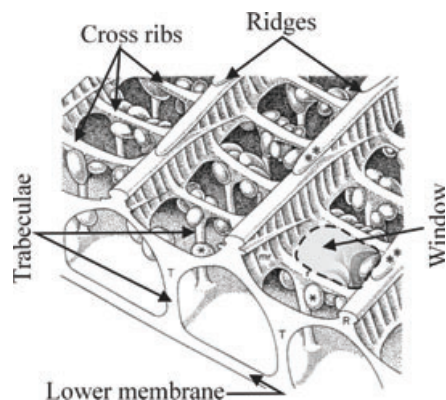


**Figure 3** Schematic structure of a butterfly scale (adapted from [38]). The lower membrane is usually unstructured, while the upper membrane has a complex nanoarchitecture in the case of scales with structural color. The very general elements of this structure are the ridges running parallel with the longer axis of the scale, the cross ribs joining them, and windows formed, through which one can see the interior of the scale. The nanostructures responsible for color can be located in the ridges, in the cross ribs, or the volume of the scale. The elongated beads in the volume are pigment granules, which are most frequently absent from scales having structural color.

as ridges running parallel with the longer axis of the scales, or cross ribs connecting the ridges. Fig. 3 shows schematically the structure of a butterfly scale. The scale arrangement resembles that of tiles on a roof, such that even wings of butterflies that appear to be only one color are in fact comprised of a ‘mosaic’, with the macroscopic appearance a result of the interaction of light with many individual scales. Moreover, the natural nanoarchitectures combine regularity and irregularity in clever ways, giving interesting optical effects that would not be possible with a completely regular structure [39].

A review of the physical colors of beetles, emphasizing the biological aspect, but including an attempt to incorpo-

rate physical models as well, was recently published [40]. In the case of beetles, the physical structures responsible for color can appear either in the cuticle itself, or in the scales [40–42]. The cuticle is a composite, with a sophisticated structure allowing for its multiple functions, one of which may be the generation of structural color. The cuticle is composed of several layers, as shown in Fig. 4 [8]. It consists of arrangements of highly crystalline chitin nanofibers embedded in an organic matrix. The structure also contains air voids, which are important for the understanding of PhC behavior, as discussed later. The color-generating layers are usually located in the epicuticle.

The recent increase in the interest of photonic nanoarchitectures in butterflies and beetles began in 1999 (Fig. 1), with the publication of a paper that presented the PhC-type structure in the scales of *Morpho rhetenor* butterflies by Vukusic et al [43]. Fig. 5 shows an image of *Morpho didius*, another equally spectacular member of the Morphidae family. Various blue-colored *Morpho* butterflies were investigated, and increasingly realistic optical models were proposed [44–51]. Numerous other types of nanoarchitectures that are different from *Morpho*-type structures occur in butterfly scales having structural color [15, 18, 26, 29, 44, 52]. A detailed classification of these structures from the point of view of biology was proposed by Ghiradella [36]. A classification of structures giving rise to structural colors in beetles was proposed recently by Seago et al [40]. In the present review, we will attempt a classification with greater emphasis on aspects relating to physics and materials science.

For PhCs with PBG in the visible, the typical size of the building elements is in the range of 100 nm and below. While the band gaps of opals and inverse opals can be conveniently computed, their practical realization is often tedious and difficult for reasons related to materials science [53] and colloidal self-assembly [54, 55]. Most other structures, which are not self-assembled, are based on sophisticated procedures such as two-photon lithography [56], three-dimensional (3D) holography [57], or direct 3D writ-

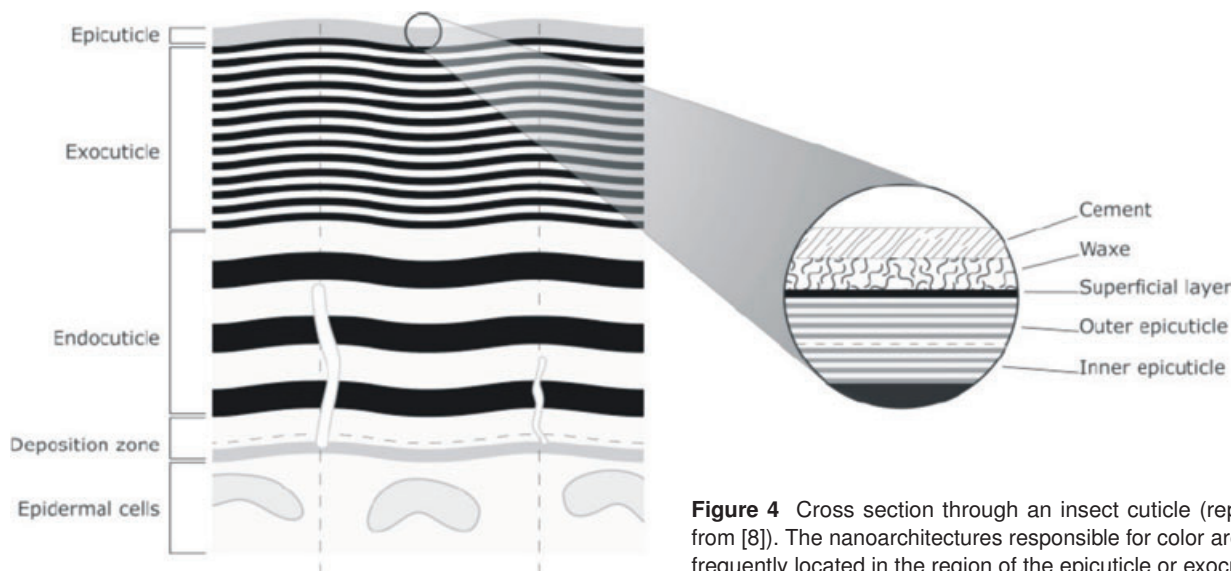


**Figure 4** Cross section through an insect cuticle (reprinted from [8]). The nanoarchitectures responsible for color are most frequently located in the region of the epicuticle or exocuticle.

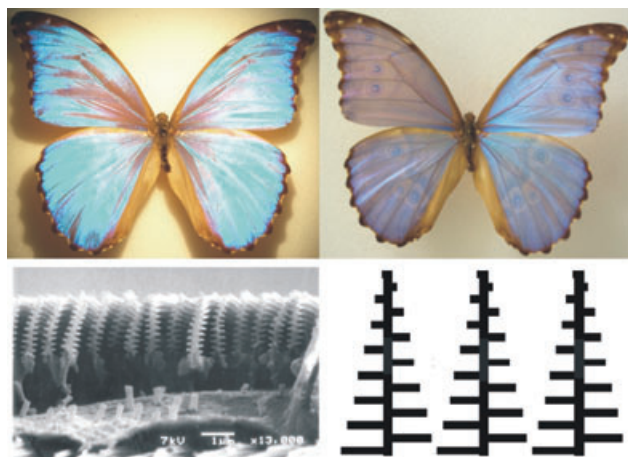


**Figure 5** (online color at: [www.lpr-journal.org](http://www.lpr-journal.org)) *Morpho didius* butterfly (top left: close to normal artificial illumination; top right, diffuse, natural illumination). Bottom left: SEM image of a broken scale of *M. rhetenor* (adapted from [46]) showing the Christmas-tree-like cross section of the ridges. Bottom right: schematic representation of the transverse cross section of the PhC constituted by chitinous material in parallel ridges and air (adapted from [45]).

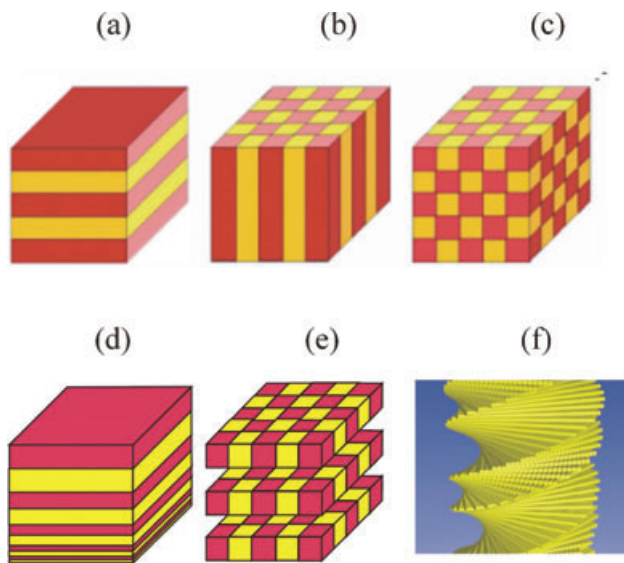


**Figure 6** (online color at: [www.lpr-journal.org](http://www.lpr-journal.org)) Schematic showing photonic crystals of a) one, b) two, and c) three dimensions (adapted from: <http://ab-initio.mit.edu/photons/tutorial/> by S. G. Johnson). Other photonic nanoarchitectures occurring in beetles and butterflies are d) chirped multilayer, e) perforated multilayer-type structure, and f) Bouligand or plywood structure.

ing [58], which presently cannot be carried out over large surfaces at practical cost levels.

A systematic analysis of technical and biological designs [59] (see Fig. 6 in [59]) shows that in biological designs, the structure dominates, while in technical designs the energy input and material complexity dominate. In biological structures, the natural variability and absence of perfect ordering is a relevant factor. Recent theoretical calculations show that in a diamond-type PhC, completely disordering the bond orientations while conserving the average particle-to-particle distance has only a slight effect on the PBG [60]. There are many examples of photonic nanoarchitectures of biological origin with various degrees of order: the rigorously ordered single-crystalline dorsal shiny metallic blue side of *Cyanophrys remus* [15], the polycrystalline structures on the mat green ventral side of the very same butterfly, and the highly disordered mat blue of the *Albulina metallica* butterfly [61] (Fig. 8).

These butterflies will be discussed in more detail later.

## 2. Photonic crystals and photonic band gap materials

### 2.1. General concepts

The concept of a ‘photonic crystal’ is often understood in a restricted sense [62, 63]. The most general concept, covering all cases, is the *graded-index periodic optical structure*, which can be defined as any non-absorbing medium which is invariant under the translations of a crystal lattice. Graded-index materials were most likely first investigated by Rayleigh, who studied acoustic waves on a string whose properties were modified by a longitudinal

standing-wave deformation [64]. The only requirement implied by the above definition is that the refractive index  $n(\vec{r})$  is real and position dependent, in such a way that a translation of the whole structure along any of the vectors  $\vec{l} = n_1\vec{a}_1 + n_2\vec{a}_2 + n_3\vec{a}_3$  (built with integer coefficients  $n_1, n_2, n_3$  on the primitive translation vectors  $\vec{a}_1, \vec{a}_2, \vec{a}_3$ ) brings no change in the optical density distribution:  $n(\vec{r} + \vec{l}) = n(\vec{r})$ . With two totally invariant directions and a discrete periodicity in one direction (such as along the  $z$ -axis), the system is a *one-dimensional graded-index periodic optical structure* (Fig. 6a). These structures are called multilayers. In the discretely periodic direction with period  $a$ , the wavevector conservation is weakened by the possible addition to the corresponding component,  $k_z$ , of any integer multiple of the quantity  $2\pi/a$ . This simple albeit important result, from group theory, drives most of the properties of waves in periodic media and will be the foundation of most of the arguments explaining structural colorations in living organisms.

When there is one totally invariant direction and two discretely invariant directions, the medium is a *two-dimensional graded-index periodic optical structure*, which is a structure made essentially of parallel fibers (Fig. 6b). In that case, only one component of the wave is strictly conserved, with the others weakly conserved (except for the addition of any of the two-dimensional (2D) reciprocal lattice vectors associated with the discrete periodicity). Finally, the full *three-dimensional graded-index periodic optical structure* shows discrete periodicity in all three dimensions of space (Fig. 6c). In this kind of structure, any incident wave with a wavevector  $\vec{k}$  aggregates 3D reciprocal lattice

vectors  $\vec{G}$  while propagating in the periodic medium. This diffraction phenomenon leads to wavevectors  $\vec{k} + \vec{G}$ .

In many cases, the graded medium consists of just two different materials separated by a sharp interface. The *interfacial periodic optical structure* can be, one-, two-, or three-dimensional. *One-dimensional interfacial periodic optical structures* define the materials from which interferential optical filters are mainly designed. The properties of multilayer stacks have been known for a long time [65, 66] and these structures are incorporated in many industrial applications today.

The properties of PhCs are related to the possible existence of a PBG, a range of frequencies where no propagation of electromagnetic waves is allowed for any polarization or direction. PBG materials have been found theoretically [67] and experimentally [68] in face-centered cubic 3D interfacial periodic optical structures [69]. Two-dimensional structures, though unable to produce a complete band gap, are also generally categorized as ‘photonic crystals’.

Many coloration structures are based on one-dimensional (1D) stacks, with small values of refractive index, typically not exceeding the refractive index of 1.8 of guanine (a material found in brightly reflecting fish scales). It is, therefore, very unlikely that a 3D *complete* gap will be found in biology. Despite this limitation, evolution has driven the coloring structures of animals to effectively use one-, two- and three-dimensional periodic structures for the common purpose of producing visual or thermal effects. The mechanism of light interference is constant and ubiquitous, and the choice to build one structure or another lies very deep in the history of animal evolution. In reality, there is no reason to look at a 1D structure with a different eye than we look at 2D or 3D structures. Likewise, there is no reason to distinguish between different regimes of refractive index values. In the context of the present review, a ‘photonic crystal’ is simply a short expression to designate one of the basic *one-, two-, or three-dimensional interfacial periodic optical structures*.

The photonic structure itself is most of the time confined to a thick layer, making a PhC film. Even if we ignore disorder for the moment, the height limitation of the structure complicates analysis. The optical functions performed by these structures can be investigated in two successive steps: the first step is to determine the dominant color produced by a given model structure and the second is to calculate the detailed reflectance spectra. Tools exist for these tasks, and we will review these in the next section.

## 2.2. Dominant reflected color: first guess formulas

Let us first consider the case of a 1D PhC with low index contrasts, along the  $z$ -direction. The multilayer film (Fig. 6a) is a repetition (a few times) of the same 1D refractive index profile. One can easily predict the location of the frequency gaps that lead to high-reflectance bands if we idealize the film by considering an infinite periodic structure and look for the occurrences of electromagnetic stop-bands. At (or

near) normal incidence ( $z$ -direction), the gap in a multilayer occurs at frequencies such that the averaged linear light dispersion line  $\omega = k_z c / \bar{n}$  meets the (extended) Brillouin zone boundaries of the 1D periodic structure. The opening of the gaps occurs at the zone boundaries; these are the only wavenumbers that can hybridize in a periodic structure, since they are separated by an integer number of  $2\pi/a$  (where  $a$  is the multilayer period). The wavelength of the reflectance bands, at normal incidence, matches the gap frequencies when the following relationship is satisfied [27]:

$$\lambda = \frac{2\bar{n}a}{m}. \quad (1)$$

In this simple equation,  $\bar{n}$  is the average refractive index in the period (obtained by spatially averaging the dielectric constant over the whole PhC film) and  $m$  is an integer chosen so that the reflected wavelength  $\lambda$  lies in the spectral interval of interest (usually, the visible range). The refractive index contrast does not influence the dominant reflected wavelength: at this level of approximation, modifying the refractive index contrast will only impact the width of the reflection band, slightly changing the saturation of the dominant color.

When the incidence is far from normal, the result must be somewhat modified in order to account for the angle-dependent relationship between the normal wavevector  $k_z$  and the frequency of light. In order to remain at the Brillouin zone boundary, the frequency must be larger than under normal incidence, in order to account for the contribution of the lateral wavevector. When the incidence angle increases, the corresponding wavelength is shifted to the blue. Translated into vacuum wavelengths, this gives the ‘iridescence rule’ [70]:

$$\lambda = \frac{2a\sqrt{\bar{n}^2 - \sin^2\theta}}{m}. \quad (2)$$

This formula is general, and it defines the wavelengths that must be totally reflected by an infinite multilayer, for any incidence angle, assuming weak refractive index contrasts. This change of color, typically from red to green, is found in many insects with a multilayer epicuticle (for instance, the ventral side of the abdomen of *Chrysochroa raja thatlandica*).

If the incidence medium is not vacuum (air), but has a finite refractive index  $n_0$ , Eq. (2) is modified as follows:

$$\lambda = \frac{2a\sqrt{\bar{n}^2 - n_0^2 \sin^2\theta}}{m}. \quad (3)$$

This formula can be applied, for instance, to marine animals with a PhC structure causing iridescence. An example of such an organism is the ctenophore *Beroë cucumis* [71]. According to the modified rule, the range of accessible colors is significantly larger for structures in water than in vacuum.

When the structures consist of a combination of multilayers with a weak periodic refractive index and inhomogeneity in the lateral directions (parallel to the interfaces), a simple formula can also be developed that accounts for the

observed sideband [72]. Following the thoughts of Rassart, we can consider a semi-infinite PhC film with a ‘vertical’ periodicity  $a$  (in the direction normal to its surface, set to the  $z$ -direction). The lateral periodicity is given by the 2D lattice vectors  $\vec{a}_1$  and  $\vec{a}_2$ , which generate the 2D reciprocal lattice vectors  $\vec{g}$ . The incident light falls along the normal, so that the incident wavevector has no lateral component. The wavevector inside the material has a normal component  $k_z$  and, due to diffraction by the lateral periodic structure, develops a lateral component  $\vec{k}_z = \vec{g}$ , which contributes to the norm of the total wavevector  $\vec{k}$ . The condition for a strong reflection is that the ‘vertical’ wavevector  $k_z$  matches one of the extended-scheme Brillouin zone boundaries. This leads to the following reflection bands:

$$\lambda = \frac{2a\tilde{n}}{\sqrt{m^2 + (ag/\pi)^2}}, \quad (4)$$

where  $m$  is an integer (1, 2, ...) chosen to fit the wavelength range of interest and  $g$  (including  $g = 0$ ) is the length of the 2D reciprocal lattice vectors. The wavelength for  $g = 0$  is essentially the reflection produced by the 3D structure when the layers normal to the coordinate  $z$  (the surface) have been averaged to produce a multilayer model, neglecting the lateral inhomogeneities. The other terms included in the equation are corrections that broaden this band towards shorter wavelengths. For large periods  $\vec{a}_1$  and  $\vec{a}_2$ , the reciprocal lattice vectors are short, and the corrections appear as a sideband on the blue side of the band.

### 2.3. Complete calculation of a photonic crystal film reflectance

The band structure of a one-, two-, or three-dimensional PhC is most often calculated in a plane-wave basis set. The Bloch theorem is applied, and the periodic parts of the electromagnetic fields are expanded in a Fourier series. The difficult part of these calculations is the slow convergence of the expansion, which forces the use of a very large number (> 1000) of reciprocal lattice vectors in the Fourier series and smoothing procedures to avoid sharp dielectric function discontinuities [73]. Maxwell’s equations reduce, for each Bloch wavevector in the first Brillouin zone, to an eigenvalue problem that produces the electromagnetic mode frequencies and the inhomogeneous material dispersion relations [74]. From these, stop-bands in specific directions can be located and the contributions to reflectance can be estimated. In a natural PhC, the refractive index contrast is never extremely large, so the calculations tend to be less demanding than for a structure based on very high index semiconductors. An interesting example of the application of the band structure calculation can be found in the work of Vukusic and Hooper [75], where the fluorescent scales of the *Papilio nireus* butterfly are investigated. In this butterfly, the fluorescent light is emitted in a 2D PhC layer on the upper structure of each scale. A band-structure calculation of the electromagnetic modes shows that this PhC structure develops a forbidden gap for light emitted parallel to

the scale surface, precisely at the fluorescence wavelength, implying the inhibition of emission in this direction. The fluorescence is then essentially directed normal to the scale surface, resulting in a very effective extraction.

Another approach of Maxwell’s equations that is very widely used is the finite-difference time-domain (FDTD) method [76]. As the name indicates, this is a field evolution scheme. One starts with initial values of the charge and current sources and the corresponding fields, and one step through time to describe the propagation of fields. From the field, the energy flow can be calculated at any point of interest. One difficulty with this approach is that the fields are represented on a special mesh (the ‘Yee’ grid) which is limited in volume. The propagating fields rapidly reach the limits of the mesh and are reflected back, unless the outer border region is a ‘perfectly matched layer’ that efficiently absorbs the outgoing radiation [77]. If spectral properties are required, it is necessary to numerically apply Fourier transforms to the time-dependent fields. The advantage of the FDTD method is that it allows for the visualization of field propagation in real space. This aids in the intuitive understanding of the succession of scattering events. The method is, however, extremely demanding on computing power. Finite-element methods allow the use of irregular grids and, because of this, are somewhat less demanding on computer resources. Today’s commercial implementations, however, essentially target radiofrequency applications.

A very successful example of the application of the FDTD method to a natural photonic structure is given by the analysis of the reflection of *Morpho menelaus* butterfly wings [78]. The scales on the wings of this butterfly have evolved (approximately) 2D ridges that produce the spectacular metallic blue characteristic of this species. The ridge structure was reproduced with rectangular elements with dimensions fitted to electron microscope observations and a scattered pulse with the frequency required to produce the needed reflectance was analyzed. An ensemble of incidence angles were considered, in order to account for incoherent scattering by the slightly fluctuating directions of the ridges, and the optical properties were very successfully compared to experimental data produced by Kinoshita et al. [46].

The last approach we will mention is the frequency-domain transfer matrix technique. This method originates in the work of Pendry on dynamical electron diffraction theory [79]. The work he developed later led to ideas that helped the implementation of a technique to solve monochromatic Maxwell’s equations [80]. A variant of this method [70] was recently used for natural structure reflectance calculations.

The whole space is divided into three distinct regions, separated by parallel planes  $z = z_I$  and  $z = z_{III}$ . These planes contain the Cartesian vectors  $\vec{e}_x$  and  $\vec{e}_y$ . The regions are as follows:

- Region I. The incidence medium, homogeneous and characterized by a dielectric constant that is real and positive  $\epsilon_I$  ( $z < z_I$ ).
- Region II. The region occupied by the PhC film. In this region, the dielectric constant  $\epsilon_{II}(\vec{\beta})$  is complex and possibly frequency dependent. It varies with the lateral

coordinates ( $\vec{\rho} = x\vec{e}_x + y\vec{e}_y$ , and with the depth coordinate  $z$ ) but remains invariant under the translations of a 2D lattice, given by the vectors  $\vec{a}_1 = a_{1x}\vec{e}_x + a_{1y}\vec{e}_y$  and  $\vec{a}_2 = a_{2x}\vec{e}_x + a_{2y}\vec{e}_y$  ( $z_I < z < z_{III}$ ).

- Region III. The emergence region, or the substrate, is homogeneous and characterized by the complex dielectric constant  $\epsilon_{III}$  ( $z > z_{III}$ ).

The objective is to evaluate the fraction of the incident energy which is reflected by the junction layer, after the infinite number of scattering events encountered within the junction layer. In order to represent the scattered field more effectively, the assumption is made, with little loss of generality, that the junction layer exhibits a 2D periodic symmetry. This may be the case when the system under study is actually periodic, but can also be used for a less restricted geometry, by defining the actual structure in a large supercell, which will ultimately be reproduced periodically. In this latter case, a convergence study must be carried out in order to determine whether the size of the supercell is large enough to overcome intercell interactions.

The technique involves first the construction of a T matrix. On each side of the inhomogeneous film, the propagation media are homogeneous and the solution is a collection of plane waves. On the incidence side, the wave is made up of all the scattered waves that are compatible with the incident waves. A ‘compatible’ wave is defined as a wave having retained the same frequency and the same 2D Bloch wavevector as the incident wave. This actually makes a quadruple infinity of field components, one for each polarization and one for each direction of propagation along the normal  $z$ -axis. The infinite numbers of beams are labeled by the reciprocal lattice vectors that we decide to keep in the problem. Maxwell’s equations, in a Fourier transform representation, easily propagate the fields from one side of the film to the other side. The T matrix serves to relate linearly the amplitudes of the quadruple infinity of the wave amplitudes in the emergence region to the quadruple infinity of the wave amplitudes in the incidence region. But if the T matrix is easily deduced from Maxwell’s equations, it does not solve the scattering problem, which seeks the outgoing waves, on each side of the film, from the ingoing waves. The matrix needed for this is called the S matrix, which can be deduced from the T matrix. However, the transformation of a T matrix into an S matrix cannot be done numerically unless the PhC film is extremely thin. Because of this, the PhC film must be cut into very thin inhomogeneous parallel layers, and an S matrix is calculated for each of these thin layers. If the assembly of T matrices is easy (this is just the product of thin-film T matrices), the assembly of S matrices is slightly more complicated, but feasible. These assembly formulas were obtained long ago by Pendry. With this tool, many types of structures in one, two, and three dimensions can be probed by simulation.

An example of an application of this technique can be found in an early paper on the *Polyommatus daphnis* butterfly, where the ‘pepper-pot’ structure was modelled using a 3D PhC film [81]. In spite of the idealization of the structure, the calculated reflectance spectrum accounts for the main features of the measured reflectance that was obtained ex-

perimentally in the same work. In this case, the calculation helped to prove that the diffuse blue colouration found on this butterfly originated from the pepper-pot structure, which was lacking in a related species, *Polyommatus marcidus*.

### 3. Order and disorder

It is very unlikely that optical engineers will learn from beetles or butterflies how to make more perfect multilayers, better dielectric or chirped mirrors. In contrast, the disorder used to achieve certain functions may be a source of inspiration.

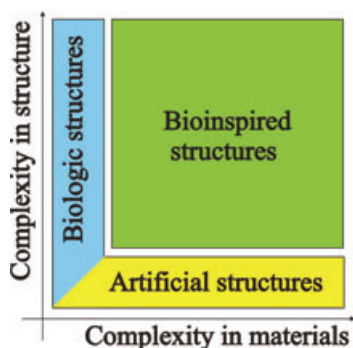


**Figure 7** (online color at: [www.lpr-journal.org](http://www.lpr-journal.org)) Schematic of the kind of complexity characteristic for artificial and biological structures and the opportunities offered by bioinspiration.

The concept of a perfect PhC, with its infinite regular order, is an idealization. Natural structures are often far from ideal, but these irregular structures remain very efficient. Moreover, there are several reasons to believe that the disorder is actually necessary. One of these reasons is the robustness of the functionality. Inaccuracies in the exact location of the scatterers do not strongly perturb the reflectance spectrum. This can be shown by perturbation [82] and it has actually been a historical argument, raised by Debye [83], that X-ray diffraction would give undisturbed diffraction directions, in spite of the disorder in atom locations induced by their thermal motion. The visual effects of slightly disordered systems tend to be more robust than those generated by perfect, ideal PhCs and this, in nature, tends to be an advantage, as variability in reproduction is one of the important features of a living organism’s evolution strategy.

Strong topological disorder also has advantages, including its influence on visual effects. Weevils and longhorns, for instance, have scales filled with scatterers that are arranged with various degrees of disorder, from nearly single-crystalline arrangements, all the way to amorphous configurations. Intermediate structures are generally polycrystalline, and the range of visual effects produced is even greater [40]. White scales (as on the weevil *Eupholus albofasciatus*) are generally composed of amorphous accumulations of spherical scatterers, while multicoloured, diamond-like scales (such as those on the weevil *Entimus imperialis*) rely on large single crystals. In between, photonic polycrystals produce metallic or mat, iridescent or stable, colorations according to the degree of disorder or the size of the PhC grains. An important point to keep in mind is that these

visual effects are reproduced from generation to generation and are well-defined traits that contribute to the characterization of an insect species. The degree of disorder is then somehow written in the genetic information attached to a species, most likely in the fabrication plan of the scales.

The disorder present in most biological nanoarchitectures is often mentioned, but generally does not receive the consideration it deserves. For example, beetle elytra have several components in the light reflected from them: a perfectly specular component and an often more significant non-specular component arising from irregularities in the structure. An example that illustrates this point is shown in Fig. 9. Both kinds of multilayers, in one case a regular multilayer (the buprestid beetle) and in the other case a chirped multilayer (*Chrysina chrysoagrea*) [40], behave in the same way. The central part of the elytra appears dark in the photograph (this indicates the absence, or negligible intensity, of diffuse illumination as compared with the direct light from light sources), and the spots where the light from the illumination sources falls under specular reflection conditions appear very bright and colorless, almost mirror-like. Large areas of the elytra, which under strictly specular conditions should appear dark, exhibit a saturated color in the case of the multilayer, or an unsaturated wideband reflection in the case of the chirped multilayer. In this later case, the silvery color indicates that the non-specular behavior is equally present for all wavelengths of the visible spectrum. The presence of color under non-specular conditions is often found in beetles, clearly indicating that the structure of the reflectors deviate significantly from those of regular or chirped multilayers. This deviation is not a secondary effect: if it were not present, the beetle would have a completely different appearance. It is worth noting that in most manmade structures, efforts are made to avoid disorder and irregularity. Biological examples show us that disorder can be useful to achieve certain optical effects, such as color visibility under non-specular conditions. A practical demonstration of this was achieved by producing a bioinspired multilayer on a sand-blasted glass substrate [27]. This very clearly demonstrates that irregularity, due to features such as substrate roughness, is not necessarily detrimental for certain applications, as beetles discovered many millennia ago (for a more detailed discussion, see Section 5.1, the case of *Crysochroa vittata*).

Similar to beetles, butterflies also have structure with disorder and irregularity that is not accidental, but instead economically adapted to the habitat of the species. For example, in the case of the forest-dwelling South American butterfly *Cyanophrys remus*, a very efficient single-crystalline PhC-based reflector is found on the scales of the dorsal side (blue, metallic color) (Fig. 8). Light is very scarce under the forest canopy, so a very efficient reflector [15] is needed for sexual communication. This butterfly usually rests on leaves with closed wings. The dorsal sides of its wings are covered by scales with randomly oriented, inverse opal-type PhCs, 5–10  $\mu\text{m}$  in size. Within each grain, a perfect crystalline structure is found. Different facets of this opal structure reflect blue, green, and yellow [15]. Due to the random orientation of the grains, a mat green texture



**Figure 8** (online color at: [www.lpr-journal.org](http://www.lpr-journal.org)) Comparison of two Lycaenid butterflies with blue dorsal color. Top: the shiny blue of *Cyanophrys remus*; bottom: the mat blue of *Albulina metallica*. The scales of *C. remus* have single-crystalline structure, while the color of *A. metallica* originates from amorphous PBG material.

is produced, which additionally does not reflect light as expected from a regular rough surface in a cone around the specular direction corresponding to the surface. Spectrogonimetric measurements revealed that most of the light is backscattered along the incident direction [15] (discussed in more detail in the next section). Another butterfly, *Albulina metallica*, realizes in some sense the ‘mirrored’ effects, mat blue dorsal color (Fig. 8) and the shiny green-gold ventral color, arising from a quasiordered layer with no long-range translational order [61]. (This will be discussed in more detail in Section 5.2.) This butterfly lives in an open, high Himalayan habitat, where it has plenty of light during the daytime, so a reflector with moderate reflectivity provides adequate sexual communication. However, due to the abundant dew in the morning hours, the grass sparkles in the sun. Against this shiny background, a mat green coloration would make the butterfly easily noticeable, so the butterfly evolved with a more appropriate, shiny color. It is worth

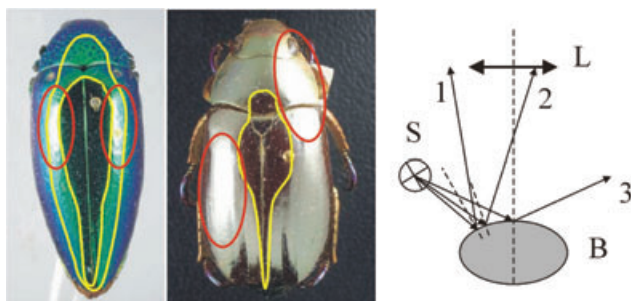


**Figure 9** (online color at: [www.lpr-journal.org](http://www.lpr-journal.org)) Non-specular behavior of insect reflectors. Left: a buprestid beetle; center: *Chrysina chrysoidea* (adapted from [40]). The regions where the specularly conditions between the light sources used and the objective of the camera are fulfilled are delineated in red. The central region of the elytra, delineated in yellow, appears dark because in that region the light is scattered under angles (beam labeled 3) that do not enter the objective of the camera (L). According to the schematic at right, if the elytra are considered specular objects, due to the curvature of the elytra, the light from regions other than those delineated in red should not enter the objective of the camera (e.g. beam labeled 1). For the buprestid beetle, the region outside of the second yellow delineation should appear black, not blue, if the elytrum behaves as a regular multilayer.

emphasizing that, to a certain degree, similar colors and similar visual effects are achieved with very different structures. This is one of the great advantages of biological evolution: it exploits random variations and their ‘fitness test’ by the environment in which the species lives. Nature can reach solutions that a rational engineer may reach only with great difficulty. Indeed, recent computer modeling of evolutionary algorithms and the way they act on the formation of photonic devices [84, 85] proves their superiority.

For a more detailed treatment of the question of regularity and irregularity in natural structural color, we refer the reader to the dedicated review on this topic by Kinoshita and Yoshioka [39].

#### 4. Principles of microscopic and optic characterization

The PBG materials generating color in the visible range are typically composed from building elements with dimensions in the 100 nm size range, or below, in one, two, or three dimensions. The most appropriate tool for characterizing relevant structural information is the electron microscope. Both scanning (SEM) and transmission electron microscopy (TEM) are very useful for providing *elements* of the needed structural information, but neither of them is able to provide complete structural information. Often, as in the case of 3D structures, even a combination of information provided by SEM and TEM images may not be straightforward [15]. SEM provides information at the surface of a specimen, revealing a topography of ridges and cross ribs (see Fig. 3). With luck, specimens can be skillfully broken in a way to probe the fractured surface with SEM, revealing information about the cross section [46, 47]. A more reliable way

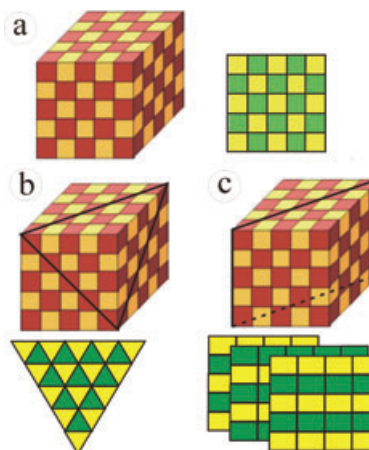


**Figure 10** (online color at: [www.lpr-journal.org](http://www.lpr-journal.org)) Schematic representation of the difficulties arising when examining one particular section of a simple model structure. Sectioned object in brown and yellow; section in green and yellow. a) Section parallel with the face of the cube (100 plane); b) section parallel with the main diagonal of the cube (111 plane); c) alternative sections parallel with the plane passing through the diagonal of the top face and of the base (110 plane).

of obtaining cross-sectional information is by using thin, ultramicrotomed sections with TEM. For this, the specimen is carefully incorporated into an epoxy block, from which thin sections are cut using a sharp, diamond knife. Unfortunately, in this procedure the precise orientation of the sectioning plane cannot be controlled, due to the very nature of preparing using a ultramicrotome thin enough sections (typically of the order of 100 nm thickness, or below) transparent for electrons.

One of the major difficulties in combining SEM and TEM data is illustrated schematically in Fig. 10. Even in the case of a very simple 3D structure such as a cube built of small cubes, and the section plane coincident with planes of high symmetry, it is not easy to deduce the complete 3D structure from information in two orthogonal planes. The reconstruction of the 3D structure is increasingly difficult for more realistic structures that are more complex and less regular. Therefore, in the case of butterfly scales, which may have rather complex geometries, using information obtained from only SEM or TEM data (and thus restricting the sampling of the object to a single plane) may be misleading [15].

One recently developed technique that has the potential to resolve the problem of characterizing a 3D structure is electron tomography. Electron tomography is a sophisticated combination of TEM imaging and computation allowing one to render an entire 3D nanostructure from a slightly thicker ultramicrotomed specimen [86]. Argyros and co-workers used this technique to obtain 3D structural information on the PhC material occurring in the green scales of the *Teinopalpus imperialis* butterfly. The technique uses thicker ultramicrotomed sections of 100, 200 and 500 nm, which are tilted inside the TEM instrument in several positions in increments of  $2.5^\circ$  over a range of  $70^\circ$  or  $120^\circ$ . In each po-

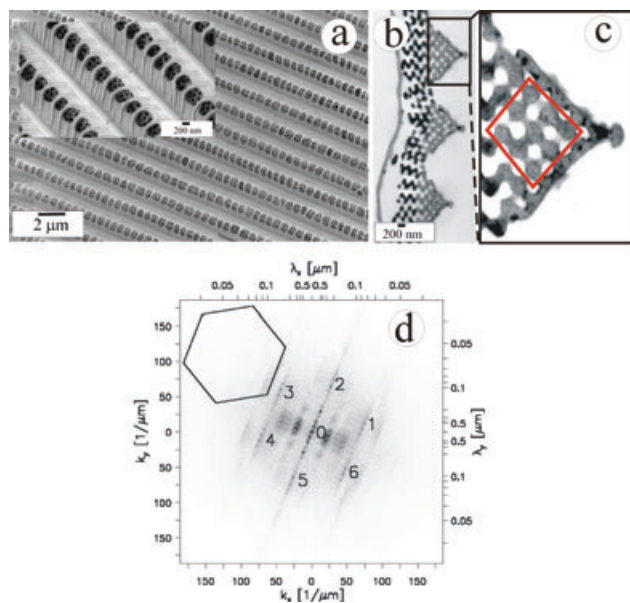


**Figure 11** (online color at: [www.lpr-journal.org](http://www.lpr-journal.org)) Electron microscope images of the dorsal cover scale of *Cyanophrys remus*. a) SEM image. The inset shows a magnified detail, in which the triangular hole pattern can be clearly seen through the windows. b) Cross-sectional TEM image, showing the PhC-type material inside the scale. c) Detail of one ridge. d) Fourier power spectrum computed from a square cut from a). The hexagon indicates the orientation of the triangular lattice of holes in a). The ridges in a) are running along the direction defined by 2–0–5. Numbers 1 to 6 correspond to maxima labeled in similar way in Fig. 12f. (Adapted from [15].)

sition, the image is recorded and dedicated software is used to build the 3D image. Experimental and computed images were compared and found to be in good agreement [86]. Unfortunately, this technique is still relatively rare and expensive.

In particular cases, when the scale can be treated as a single crystal with long-range translational order, such as the dorsal side of *Cyanophrys remus*, it may be possible to accurately reconstruct the structure from SEM and TEM images (Fig. 5 in [87]), which can subsequently be crosschecked by computer simulations to see if leads to the observed optical effects [15]. Prior to attempting the reconstruction, one has to make sure that the scales are indeed of single-crystalline character. This can be achieved by calculating the Fourier power spectrum of the electron micrographs [15]. However, the interpretation of the Fourier spectrum of complex images is typically not straightforward. In Fig. 11, experimental SEM and TEM images are shown, together with the Fourier spectrum of the SEM image. The reconstruction of the Fourier power spectrum is shown in Fig. 12, and the reconstruction procedure itself is discussed in detail in [15]. Comparing Fig. 11d with Fig. 12f confirms that the Fourier power spectrum obtained from the experimental SEM image is a result of the convolution of the elementary structures presented in Figs. 12a and b. In other words, the triangular pattern of small holes that can be seen through the rounded, rectangular windows do in fact possess single-crystalline, long-range order.

Fourier analysis is a very convenient tool when structures exhibiting long-range order are present. A method using a different approach, but also using the Fourier power spectrum interpretation of cross-sectional TEM images, has been applied by Prum et al. to butterfly scales [88]. They had previously used a similar method to correlate structural and spectral data of quasicrystalline PhC-type structures in avian [89] and mammalian skin [90]. The extension of this color-generation mechanism from insects to birds and mammals indicates that the mechanism was ‘rediscovered’ by evolution in several different cases.

The optical characterization of butterfly scales and beetle elytra should be carried out with caution. As can be easily deduced from Fig. 3, the individual butterfly scale is itself a complex enough object to behave non-specularly. Moreover,

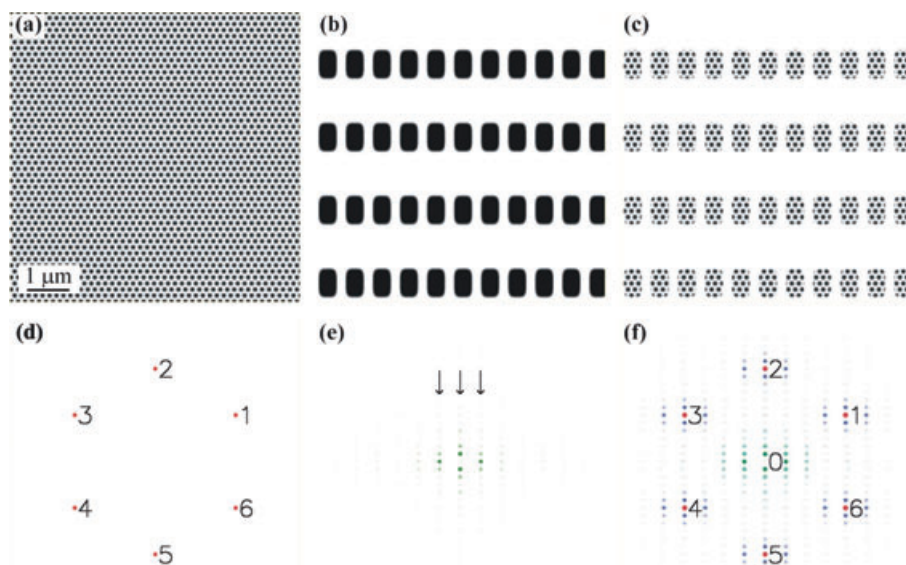


**Figure 12** (online color at: [www.lpr-journal.org](http://www.lpr-journal.org)) Reconstruction of the Fourier power spectrum from Fig. 11d. a) Triangular hole pattern (seen through the windows in the inset of Fig. 11a); b) the pattern defined by the windows; c) structures resulting from overlapping b) and a); d) Fourier power spectrum of a); e) Fourier power spectrum of b); f) Fourier power spectrum of c). (Reproduced from [15].)

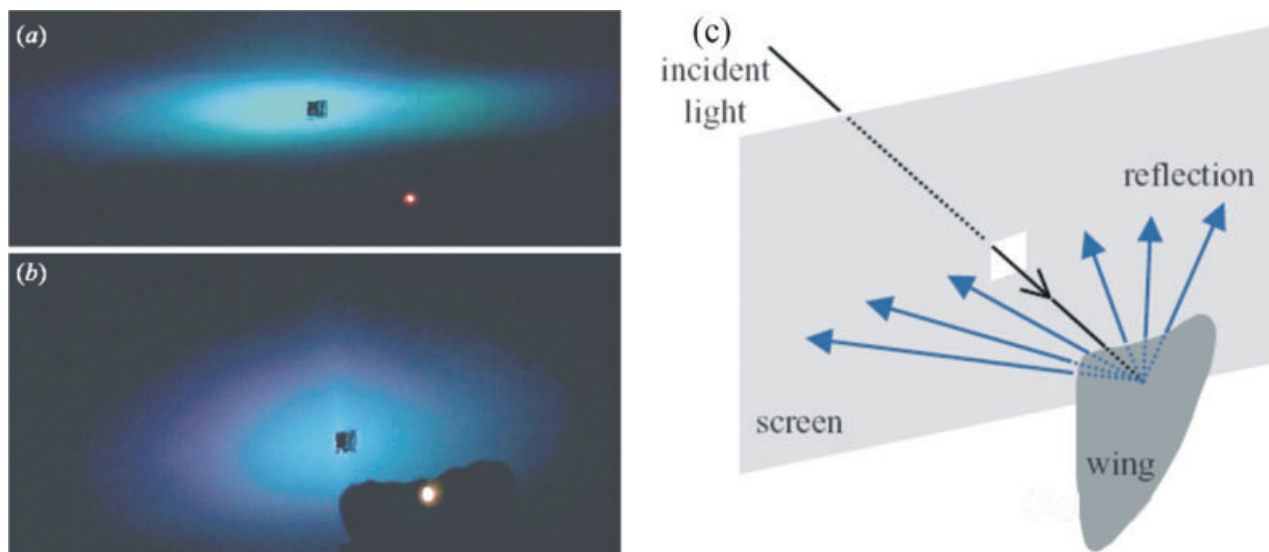


**Figure 13** (online color at: [www.lpr-journal.org](http://www.lpr-journal.org)) Light scattered by blue *Morpho* wings. a) *Morpho rhetenor* wing; b) *Morpho didius* wing; c) schematic representation of the experimental setup used (adapted from [92]). One can clearly notice the non-specular character of the light scattered from the wings. The scattering patterns are different and characteristic for the two butterflies.

even the ridges within one scale, in scales with ordered aspect, like in the case of *Morpho* butterflies, may behave as individual optical objects [39]. This is accentuated by the fact that a butterfly wing is composed of several layers of scales and these scales are oriented at a certain angle with respect to the wing membrane [91]. In the case of beetles, the deviation from specular behavior also frequently has to be taken into account, as demonstrated by Fig. 9. The lack of specular behavior means that characterization using standard reflectance measurements may be misleading. This is very convincingly demonstrated by a simple scattering experiment reported by Yoshioka and Kinoshita [92]. They used a white screen with a small hole to observe the angular spread of the light scattered by a *Morpho* wing and a single scale (Fig. 13). If an experimental setup only allows specularly reflected light to enter the detector, it will miss a significant fraction of the reflected light.

Another, more quantitative way of handling non-specular behavior is to use a spectrogoniometric setup as shown in Fig. 14. A simple spectrogoniometer is built from a commercial fiber optic spectrometer and a gonimetric stage, which allows the precise positioning in the upper hemisphere of the illumination and pick-up fibers with respect to the specimen. The detailed spectral characterization of the dorsal and ventral side of the *Cyanophrys remus* wing using such a spectrogoniometer is reported in [15]. Another useful instrument developed recently by Stavenga and co-workers is the imaging scatterometer. This instrument allows one to obtain a photographic representation of the characteristic scattering pattern for a butterfly wing [52]. As *C. remus* and *C. rubi* are known to have similar nanostructures in their ventral cover scales [15, 35] and the macroscopic aspect of the wings as well as low-magnification optical micrographs are very similar [15, 52], they offer a perfect opportunity to compare results obtained using the imaging scatterometer [52] and spectrogoniometer [15] (Fig. 15). Both techniques reveal a

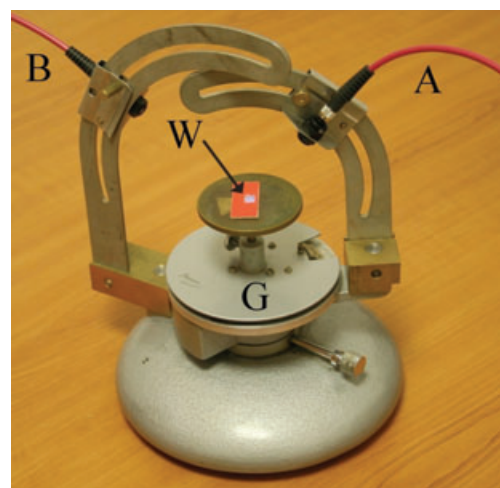


**Figure 14** (online color at: [www.lpr-journal.org](http://www.lpr-journal.org)) A simple spectrogoniometric setup using a commercial fiber optic spectrometer (not shown) and a gonimetric stage: A, illumination fiber; B, pick-up fiber; G, gonimetric stage; W, piece of framed butterfly wing. The arcs supporting fibers A and B can be rotated 360°.

strongly non-specular behavior. According to the spectrogoniometric measurement, under a 45° incidence on the wing plane, the intensity of the specularly reflected light is of the order of 15%, regardless of the azimuthal rotation angle (the azimuthal rotation gives the variation of the incident plane with respect to the direction ridges in the plane of the wing). The intensity of the backscattered light is around 70%. The imaging scatterometer shows that the illumination falling close to normal onto the wing is uniformly scattered in all directions around the incident direction in a cone with an opening exceeding 60°, while the spectral position of the maximum is not changed [52]. The same imaging scatterometer was used to investigate the light reflected from

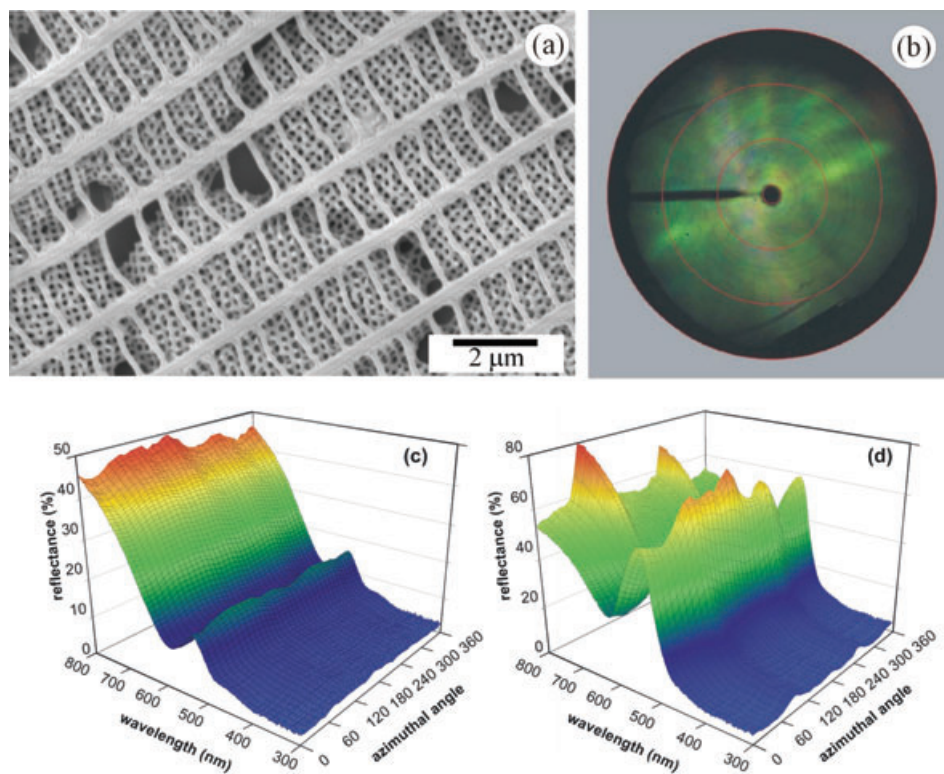


**Figure 15** (online color at: [www.lpr-journal.org](http://www.lpr-journal.org)) Microstructure and light scattering from the polycrystalline, inverse opal structure of *Cyanopryus remus* and *Callophrys rubi*, known to have similar microstructures. a) SEM micrograph of a ventral (mat green) cover scale of *C. remus*; b) scatterometer image of light scattered from a ventral scale of *C. rubi* (adapted from [52]); c) light scattered in specular direction under a 45° angle of incidence from the ventral side of *C. remus* wing; d) light backscattered under a 45° angle of incidence from the ventral side of *C. remus* wing.

individual scales and wing pieces of *Morpho aega*. In accordance with earlier results [43,92], it was found that the angle of scattering is moderate in a plane parallel with the ridges of the scale and strong scattering occurs in a plane normal to the ridges.

These experimental data show that a suitable apparatus for detailed optical investigation of naturally occurring PhCs and for their artificial counterparts would be an optical instrument similar to the X-ray diffraction instruments, but operating with tunable lasers. Of course, integration spheres can be used to collect light that is scattered under non-specular angles [61, 93]. Unfortunately, when using such a sphere, valuable information regarding the angle of scattering is lost. In addition, components of multiple diffuse reflections from internal surfaces of the sphere are directed back at the sample at a range of different angles. This leads to a convoluted reflection from the sample, comprising components of many different angles [94].

## 5. Examples of natural photonic nanoarchitectures

### 5.1. One-dimensional structures

One-dimensional structures, or multilayers, if understood in a wide sense, are the most widespread photonic nanoarchitectures occurring in the living world. They are responsible for the colors of many beetles and butterflies. However, realistically, none of these biological nanoarchitectures are actually 1D structures in the strict sense of the word. Rigorously speaking, a 1D structure should behave in a perfectly

specular way, as do artificial multilayers. On the other hand, if a color is used for communication in the living world, it could be rendered useless by such a limited viewing angle. Therefore, imperfect natural nanoarchitectures benefit from the color selection mechanism of 1D structures, but also modulate the angular spread and the intensity of the signal with disorder. As discussed above in some detail, the *Morpho*-type scales exhibit a very different magnitude of the angular spread in the plane parallel or perpendicular to the plane of the scale's ridges. *Morpho didius*, for example, has special transparent cover scales, which widen the angular spread of the color generated, opposite to the usual way by the ground scales [47]. Nevertheless, most groups model *Morpho*-type scales with 1D structures [43, 46–48, 95]. A more complex treatment of the color generation of *Morpho*-type scales was given by Gralak et al [45]. They modeled the scale structure with the help of a rigorous lamellar grating electromagnetic theory. In this way, they were able to determine the colors reflected by the wing under various illumination conditions. Recent modeling and experimental work by Plattner [49] showed that in fact the investigated *Morpho*-type scales show efficient low-pass filter behavior for all angles of incidence and polarizations, with near-complete transmission at wavelengths above a threshold of 550 nm. The angular spread of the backscattered light was found to be organized in lobes with total extinction of the specular reflection for all conditions of incidence. Retro-reflector behavior was also observed for angles of incidence of 30° and above. All of these findings, in accordance with earlier [43, 96] and more recent results [32, 52], show that, in fact, the behavior of *Morpho*-type scales is much more complex than a simple multilayer theory predicts. Neverthe-



**Figure 16** (online color at: [www.lpr-journal.org](http://www.lpr-journal.org)) SEM images of male *Hoplia coerulea* head, covered by scales (left) and the interior of a fractured scale (right). The inset shows *H. coerulea* male on a green leaf. (Adapted from [99].)

less, the color selection rules can be satisfactorily deduced with 1D multilayer theory.

The shiny, metallic color, silver, or gold aspect of many beetles can be attributed to 1D photonic structures [27, 40, 94, 97–101]. In a simple, but very convincing experiment, Hariyama et al [98] proved in the case of various colored *Plateumaris sericea* beetles that although both the epicuticle and the exocuticle have a multilayer structure, with the number of layers significantly higher in the exocuticle region, only the epicuticle contributes to the color. When the epicuticle was mechanically removed, all beetles, regardless of the initial color, appeared black.

Vigneron et al [99] investigated *Hoplia coerulea*, which similarly to butterflies has scales that generate the blue-violet color of the beetle. Inside these scales is a multilayer-type structure. The blue iridescence is shown to originate from the structure of the squamae within scales, shown in Fig. 16. The internal structure of the scales shows a stack of planar sheets, separated by a well-organized network of spacers, a structure that belongs to the family of the multilayer (1D) PhCs. In this case the multilayer is constituted of filled chitin layers and layers filled partially by chitin and partially by air. Such a structure, after infiltration and sectioning for cross-sectional TEM preparation, should have ‘electron absorbing’ layers (originally chitin) alternating with ‘less electron absorbing’ layers (originally air and chitin). The presence of spacers will be unambiguously visible. The blue iridescence is explained by a planar multilayer approximation model, which is deduced from the observed 3D structure, and idealized as a 1D multilayer. First, a simplified model is applied to estimate the color of the multilayer at normal incidence [99]: using Eq. (1), with a period  $a = 160$  nm as determined from SEM images and an average refractive index  $\bar{n} = 1.4$  calculated from the filling of layers, and  $m = 1$ , one gets a wavelength of 448 nm, which is in good agreement with naked eye observation and reflectance measurements. More detailed computations were carried out using a transfer matrix approach confirming the validity of the simple model.

Another somewhat unusual multilayer structure was found in the cuticle of *Chrysochroa vittata* [27] (Fig. 17a). Careful SEM investigation revealed that the cuticle is built of chitin layers 204 nm in width, separated by layers of air and irregular corrugations on the sides of the bulk chitin layer with a height of 10 nm. The amplitude of these irregularities determines the air spacing between the chitin sheets.

The size and shape of this separation layer contributes to the reflectance bandwidth, and not to the dominant wavelength. This multilayer structure is rather different from the usual artificial structures where equal or at least comparable layer widths are used for the high and low refractive index layers. This unusual structure will have a role in the production of a bioinspired artificial layer, discussed in more detail later. Using Block’s theorem, it is possible to derive a formula for describing the wave propagation through such a structure constituted of layers of very unequal thickness [27]. Using Eq. (2), only  $m = 1$  gives rise to a visible reflection band, which occurs at the wavelength  $\lambda = 627$  nm. A red coloration is indeed observed at normal incidence on the ventral side of *Chrysochroa vittata*, from which the cuticle sample was taken. At a grazing incidence of  $\theta = 75^\circ$  as in the experiment, the model leads to a dominant wavelength of 488 nm for transverse electric (TE) polarization and 472 nm for transverse magnetic (TM) polarization. This shift is easily observed when looking at the insect from the side or rear: the ventral side of the insect’s abdomen displays, to the naked eye, a bluish-green coloration. More exact results can be obtained by computing the reflectance spectra of the chitin/air multilayer, calculated from an exact solution of Maxwell’s equations by a transfer matrix method [27] (Fig. 17).

Certainly, a critical issue in modeling and computing the optical properties of beetle elytra is the question of the refractive indices to use. Recently, Noyes et al [94] used detailed optical measurements and modeling to propose that, in the case of the buprestid beetle *Chrysochroa raja*, the complex refractive indices of both layer types (high index and low index) are:  $n = 1.68$ ,  $k = 0.03$  and  $n = 1.55$ ,  $k = 0.14$ . The  $n$  values of the two layers are surprisingly similar. Layer thicknesses were measured from TEM images after a staining procedure. Possible deviation of the sectioning plane from the plane normal to the multilayer, or sample deformation during ultramicrotoming cannot be excluded. Another possibility is that *C. raja* also has corrugated chitin layers like *C. vittata*, in which case the TEM sections may be difficult to evaluate precisely. Noyes et al [94] give a critical overview of refractive index values used by other authors.

A rather intriguing case is that of *Charidotella egregia* [100], a tortoise beetle that is able to change its golden structural color to red when disturbed (Fig. 2). The beetle can typically perform this color change in about a minute. Optical and other physical measurements, in combination

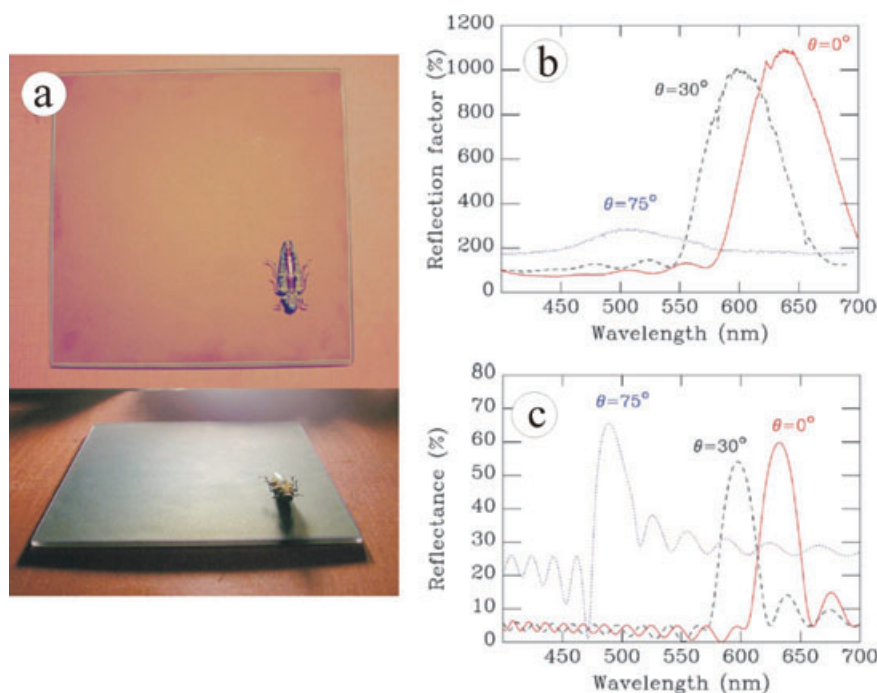


**Figure 17** (online color at: [www.lpr-journal.org](http://www.lpr-journal.org)) *Crysochroa vittata* on an artificial bioinspired multilayer. a) Sandblasted glass plate with a multilayer produced according to the blueprint of *C. vittata* cuticle. Note the corresponding colors of the insect and the artificial multilayer. b) Experimental reflectance of the insect cuticle. c) Computed reflectance of the multilayer structure revealed by SEM in the cuticle. (Adapted from [27].)

with modeling and computer simulation, revealed [100] that the color change is made possible by a chirped multilayer (Fig. 6d) in which one of the constituting layers is porous. The insect can pump body liquid in and out of the porous layers. In the filled condition, the porous layers are an optically homogeneous, transparent medium, with an effective refractive index different from the solid layers, and thus building up a chirped multilayer. In this status, the epicuticle appears shiny and golden, as it reflects all visible wavelengths with the exception of the blue range. When the pumping is stopped, the porous layers lose the liquid, and they become an optically diffusive medium that disrupts the chirped multilayer. The red pigment color lying deeper in the structure becomes visible. Chirped multilayers, rather than switchable ones, with silver or gold aspect are reported in the beetles *Chrysina chrysoagryrea* [40] and *Anoplognathus parvulus* [97], and in the pupa of the *Ideea leucone* butterfly [39].

## 5.2. Two-dimensional structures

At our present level of knowledge, 2D nanostructures, as depicted in Fig. 6b, occur less frequently in the color generation of beetles and butterflies than their 1D and 3D counterparts. A very nice case of a 2D structure is presented by Yoshida [102]: a regular-hexagonal array of conically shaped protuberances in the scales and transparent wings of *Cephonodes hylas* (Fig. 18). However, this structure does not generate color, but instead acts as an antireflection layer, akin to an optical ‘index matching’ layer with a continuous increase in the effective refractive index as the filled fraction increases towards the wing membrane. Mechanically crushing the dot matrix increased the wing’s measured reflectance by between two and three times [102].

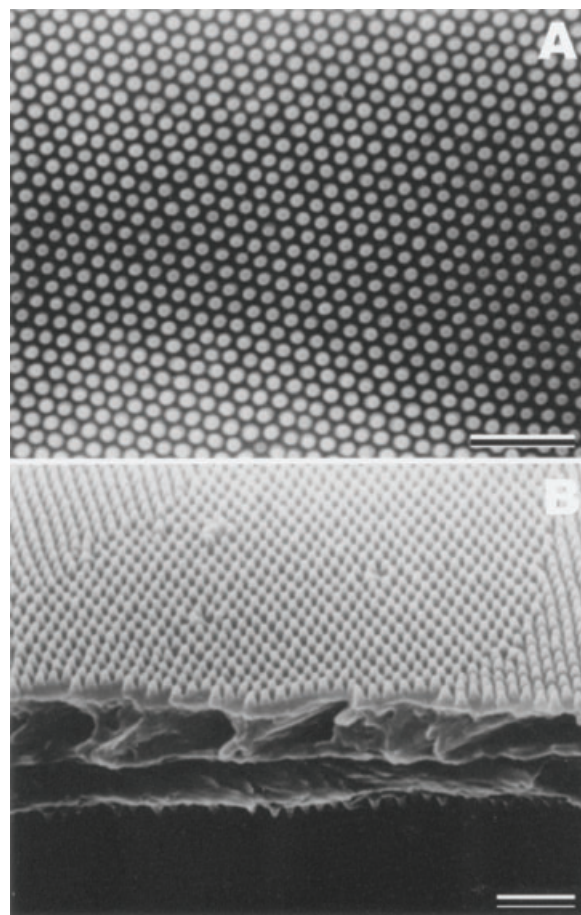


**Figure 18** Protuberance array in the *Cephonodes hylas* wing. A) SEM micrograph of the upper view of the wing (scale bar: 1 μm). B) SEM micrograph of the oblique view of the wing, cut with scissors (scale bar: 1 μm). (Reproduced from [102].)

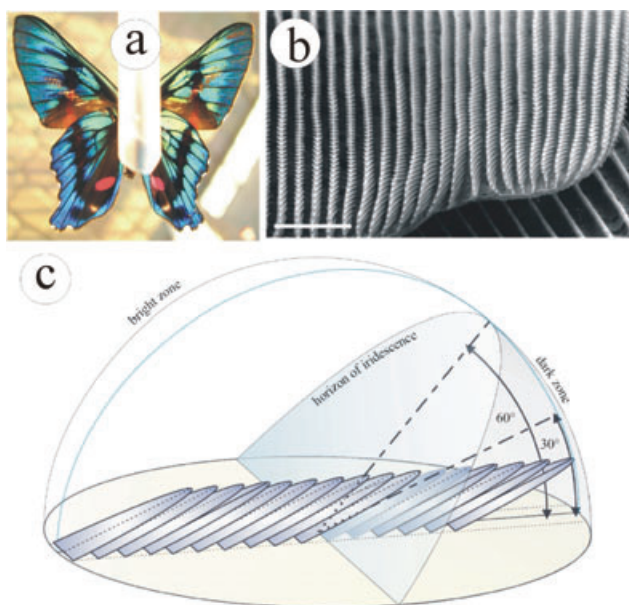


**Figure 19** (online color at: www.lpr-journal.org) Color and scale structure of the *Ancylyuris meliboeus* butterfly. a) *A. meliboeus* photographed in natural light. The butterfly is pinned to a thin plastic tube to facilitate manipulation. b) Scale structure as revealed by SEM (scale bar: 3  $\mu\text{m}$ ) and c) structural model of a single lamellar ridge (reproduced from [103]).

In a broader sense, several 2D structures occur in butterfly scales that can be equally regarded as 2D PBG materials or 2D diffraction gratings (bi-gratings). For example, the scale structure of the South American *Ancylyuris meliboeus* butterfly can be regarded as a 2D structure [103]. The ridges running along the longer axis of the scale have a lamellar structure, as shown in Fig. 19. In a rather unusual way, in the case of this butterfly the ventral side of the wing exhibits a very bright iridescent color composed of different hues of blue, green, and yellow. Due to the slanted orientation of the lamellae in the ridges at  $60^\circ$  with respect to the plane of the scale, the iridescence is visible in a limited angular range, which happens to be different on the left-right and fore-hind wings. Therefore, the photographic rendering of the full beauty of this butterfly is not possible. The visual effects were explained by Vukusic et al [103] as diffraction occurring concurrently with interference. They used a bi-periodic model in real space in which the cross section through the ridges of the scales was represented as a section of a 2D photonic crystal. This structure produced bright structural color in a limited angular region over the ventral wing surface, enabling a remarkably strong flicker and color contrast with minimal wing movement. The visibility effects associated with its color, in terms of bright and dark zones of the observation hemisphere over the wing surface, were described. The observed colors were successfully modeled using a double diffraction grating model and Ewald sphere approach, commonly used in the modeling X-ray diffraction in crystals [103].

In a certain sense, a similar structure was revealed in the scales of the *Troides magellanus* butterfly [18, 104] that

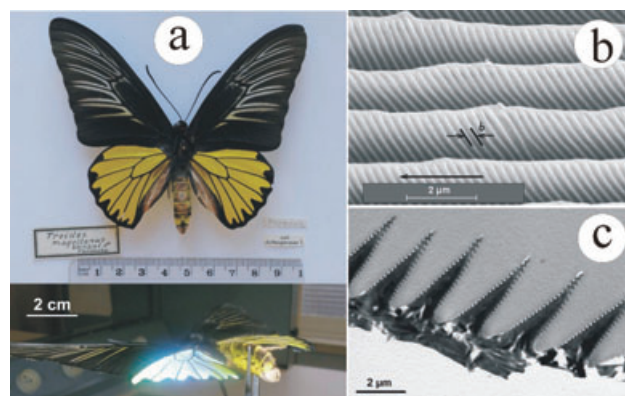


**Figure 20** (online color at: www.lpr-journal.org) *Troides magellanus* butterfly and glancing angle view, and scale nanoarchitectures. a) Diffuse daylight illumination image of *T. magellanus* (top) and glancing angle view photograph taken with flash illumination (bottom). The whitish-blue color is due to combined diffraction and fluorescence. b) SEM image of ridges with slanted lamellae. c) Cross-sectional TEM image of triangular ridges. The lamellae are visible as small protrusions on the sides of the ridges. (Reproduced from [18].)

lives in a very restricted region in Indonesia and a small island southeast of Taiwan. The scales of *T. magellanus* also have ridges with lamellae positioned at a  $60^\circ$  slant [18, 104] (Fig. 20). The triangular body of the ridge is filled with papiliochrome II, giving the wings their yellow color. This fluorescent pigment has an important role in the optical aspect of the butterfly. Two, slightly different descriptions of the diffraction have been given: Lawrence et al [104] use a bi-grating model, while Vigneron et al. use a blazed diffraction grating model [18]. The latter model is able to account for the enhancement effect in the fluorescence of the yellow pigment observed under diffraction conditions.

An unusual optical effect arises from two independent diffraction gratings in the cover scales of the hind wings of the males of the *Lamprolenis nitida* butterfly. Two different patterns of iridescence are visible from opposite directions: a bright red to green iridescence is seen anteriorly, while a weaker, violet to ultraviolet reflection is visible posteriorly [105]. The cross ribs of the scales have a lamellar shape and are oriented at an angle of  $30^\circ$  with respect to the scale plane, while a second diffraction grating is formed by the flutes on the sides of the ridges. While the cross ribs give rise to a red-green iridescent color, the flutes produce the violet-UV color.

The diffraction grating-type structures in beetles have been reviewed recently, and we refer the reader to Seago et al [40] for more information.

Two other cases of color-generating nanoarchitectures can be included in the category of 2D structures: the sculpted multilayer structures that occur in beetles [29, 106–109] and the various kinds of perforated multilayers that occur in butterfly scales [61, 81, 109–111], in particular Lycaenid butterflies. Neither of these is a 2D structure in the strict sense of Fig. 6. Comparing Figs. 6b and e shows that the structure in Fig. 6e can be regarded as a transition between a 2D and

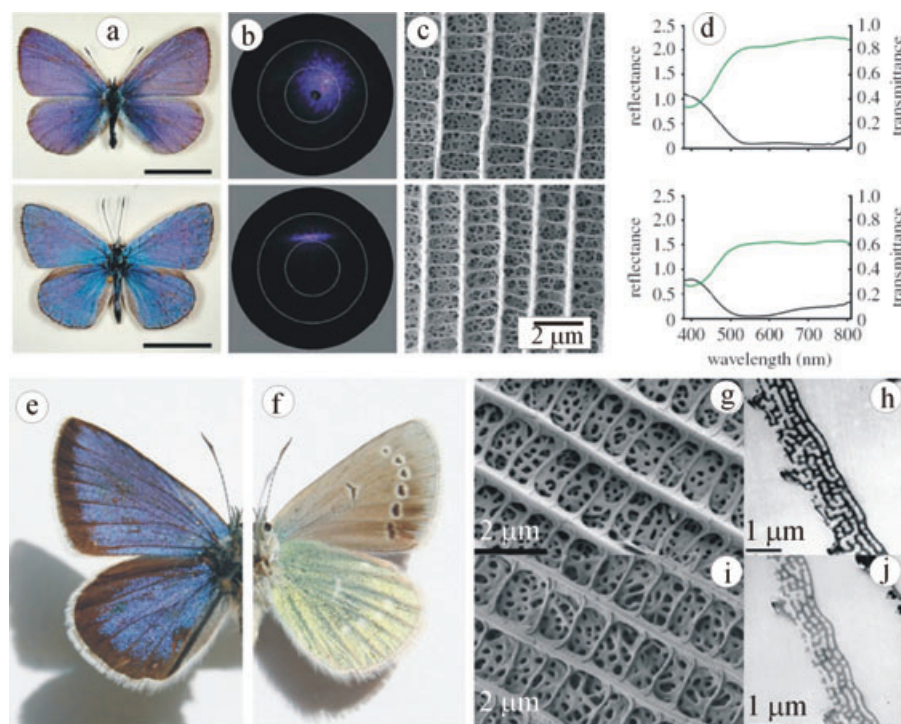


**Figure 21** (online color at: [www.lpr-journal.org](http://www.lpr-journal.org)) Lycaenid butterflies with perforated multilayers in their scales. a) Photograph, b) scattering pattern, c) SEM micrograph, and d) reflectance and transmittance data for *Celastrina argiolus* (top) and *Polyommatus icarus* (bottom). Note the very different scattering patterns of the scales, looking similar in the SEM images. (Reproduced from [110].) *Albulina metallica* e) dorsal and f) ventral view; g, i) SEM and h, j) TEM micrographs of the scales (g, h, dorsal side; i, j, ventral side). The scales exhibiting similar nanostructures generate different colors. (Adapted from [61].)

a 3D structure. Recently, Stavenga and co-workers [110] carried out a systematic investigation of several Lycaenid butterflies with a simplified version of the imaging scatterometer mentioned previously [52]. An illumination spot 10  $\mu\text{m}$  in diameter was used on single scales; the light that is backscattered from the scale is focused in the second focal point of an ellipsoid mirror, which coincides with the focal point of a camera objective lens. The far-field radiation pattern of the object thus emerges in the back focal plane of the lens. This plane is subsequently imaged on the photosensitive chip of a digital camera. The obtained image slightly deviates from a polar diagram [110], but very clearly shows that most of the investigated nanoarchitectures have a non-specular scattering pattern. The light incident along the surface normal was most frequently scattered at angles exceeding  $30^\circ$ , in patterns of varying shape. As seen from SEM images and as discussed in more detail by Stavenga and co-workers, the scales consist of layers with different degrees of perforation. However, as pointed out earlier, the SEM images give information only about the structure of the topmost layer. As one can observe in Figs. 21a–d, the two kinds of nanoarchitectures look similar in the SEM images and have similarly placed reflectance maxima in the spectra, but give very different scattering patterns. On the other hand, *Albulina metallica*, also a Lycaenid butterfly with scales of similar nanomorphology, generates a blue color on the dorsal and a green color on the ventral sides of its wings. SEM and TEM micrographs (Figs. 21h and j) both show that the blue and green scales of *A. metallica* are composed of several layers with a quasiordered distribution of perforations. Using a direct space averaging technique [26], it was shown that in the topmost layer of the blue and green scales the average hole distance correlates with the position of the reflectance maximum. These experimental data show

that the color selection of the nanoarchitectures in the scales of the Lycaenid butterflies discussed can be regarded as 2D. On the other hand, important properties like the direction and angular spread of the scattered light and its intensity may be influenced by the structure and scattering of deeper lying layers as well. The work of Prum et al [88] in which a 2D Fourier power spectrum was used to show correlation between the distribution of holes in cross-sectional TEM images of butterfly scales and their measured color supports this interpretation. In other words, there are clear signs that the optical behavior of this type of scale is decided by the structure of the scale in more than one relevant dimension. Further experiments may be needed to decide if the behavior is closer to 2D or 3D. A model that is closer to a 3D structure was used to reproduce the color of *Polyommatus daphnis* butterflies [81]. This model is constituted of layers of parallelepipedic voids, separated by a rectangular network of chitin walls. The specific dimensions were extracted from SEM images. The individual layers are shifted by one half period with respect to the upper and lower neighboring layers. The calculation of the reflectance of this layer has been performed using a transfer-matrix approach, both for the square-shaped air boxes and for a structure in which the rectangular voids have been replaced by hollow ellipsoids. Both calculations yielded a reflectance maximum at 470 nm, in good agreement with experimental value of 490 nm [81]. The shape of the cavities affected the reflectance in the spectral range of 550–700 nm.

The sculpted multilayers differ from the 1D structures discussed previously (Section 5.1) by the presence of ‘dimples’ in the color-generating multilayer. The topography of the multilayer structure (with 1D periodicity on the 100 nm scale) follows the profile of these dimples (with distances on the micrometer scale), as shown in Fig. 22. This is equivalent

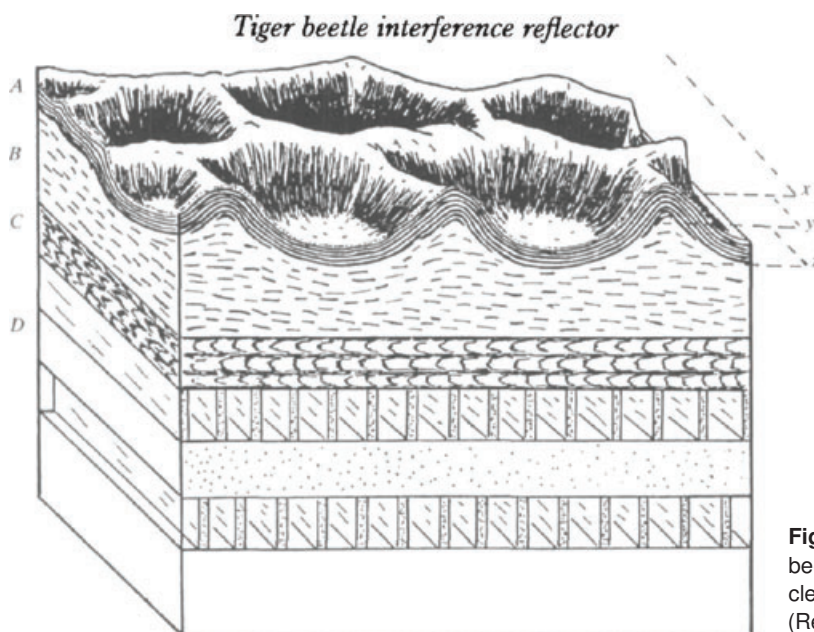


**Figure 22** Schematic structure of the cuticle of tiger beetles as proposed in [88]: D, endo- or mesocuticle; C, inner exocuticle; B, outer exocuticle; A, xxx. (Reproduced from [106].)

to a 2D modulation of the multilayer, but the characteristic length scale of the 2D modulation is much larger than the layer periodicity, which is responsible for the color selection of 1D structures. For this reason, such a structure is not considered to be a 2D structure in the strict sense. As the angle of incidence is significantly different in the deepest region of the dimple and on the sides of the dimple, the multilayer periodicity encountered by incoming light will also be different. On the sides of the dimple, the blue-shift of the reflected wavelength found in 1D structures at shallow incidence will be present. This may be used in many ways: for better crypsis [40], for inconspicuous appearance [107], etc. Similar structures with similar behavior were also reported in butterfly scales [29, 112, 113].

### 5.3. Three-dimensional structures

Two examples of the 3D nanoarchitectures occurring in butterfly scales have been discussed above: the blue and green cover scales of the male *Cyanophrys remus* [15]. While the nanoarchitecture of the dorsal blue scales is less frequently described in recent papers – Berthier et al. report a possibly similar structure in *Suneve coronata* scales [29] – the inverse opal-type polycrystalline structure of the ventral green scales is fairly often encountered [35, 37, 86, 88, 114, 115]. Scales of this structure have been reviewed recently under the generic name of gyroid structures [116]. It is worth noting that to date, all reported cases of the inverse opal type-structures in butterfly scales are associated with a green color: *Cyanophrys remus*, ventral scales [15], *Parides sesostris* [88, 114, 116], *Mitoura gryneus* [37, 39, 88], *Callophrys rubi* [35, 88, 116], *Teinopalpus imperialis* [86, 115], *Troides priamus* [88], *Thecla imperialis* [115], and *Udara blackburnii* [115]. This may be linked to the value of the refractive index contrast between chitin and air. Interestingly enough, theoretical modeling has shown from photonic band

and electric field power profile investigations in inverse opals that feasible PhC-based devices using low index materials could result in larger full PBGs in the visible [117]. On the other hand, even an incomplete gap is perfectly sufficient for the color generation of living organisms. Another simple explanation may be that because it is well known that green pigments are absent in butterfly scales, green-colored butterflies were preferentially examined.

The nanoarchitectures that occur in beetles and clearly belong to the 3D group are most frequently also of a direct opal, or inverse opal, type. An opal analogue was reported in the scales of the weevil *Pachyrhynchus argus* by Parker et al [118]. Later Welch and Vigneron showed a full ‘spectral range’ of weevils from blue to red [119]. In the scales of the *Pachyrhynchus congestus pavonius* weevil (Fig. 24), an inverse opal-type polycrystalline nanoarchitecture was found, giving an orange color [120].

Recently, in another weevil, *Lamprocyphus augustus*, a diamond-type 3D lattice was found using focused ion beam milling and model calculations [121]. As in the other weevils discussed previously, weevil scales have a polycrystalline structure and produce a green color with little angular dependence. SEM images reveal a diamond-type structure, one of the more general gyroid-type structures [116].

### 5.4. Bouligand-type structures

A special case of 3D structures is the Bouligand, or plywood-type, structure (Fig. 6f) that is frequently found in scarab beetles (Coleoptera: Rutelidae, Cetoniidae). It is composed of fibrils arranged in layers in such a way that the fibril orientation changes circularly from layer to layer. A pitch  $p$  can be defined as the distance in a direction normal to the layers after which the same orientation of the fibrils is found again. Such structures were described quite early on by Neville and Caveney [122], and were compared to the cholesteric

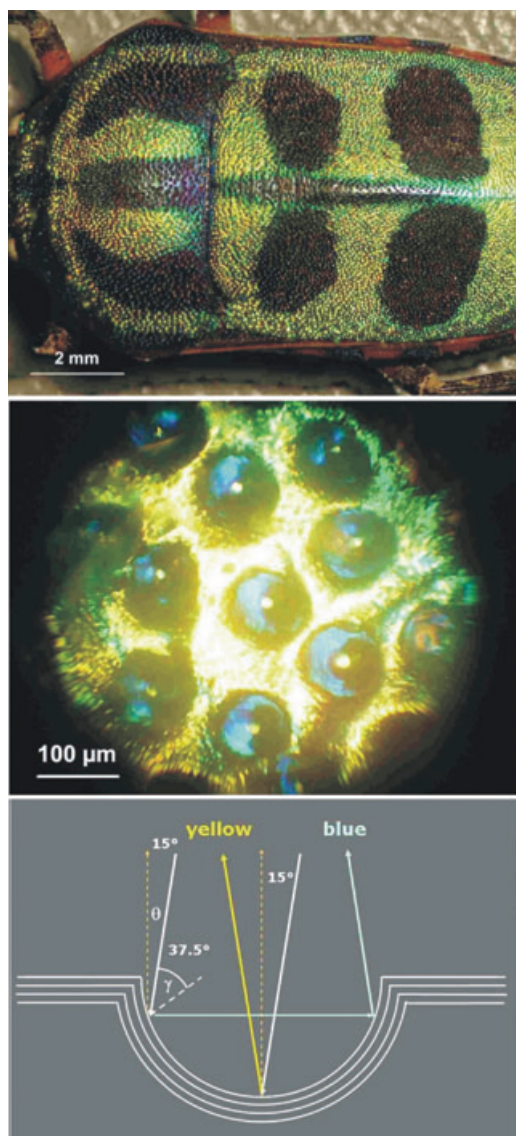


**Figure 23** (online color at: [www.lpr-journal.org](http://www.lpr-journal.org)) African shield-backed bug *Calidea panaethiopica*. Top: macroscopic view; centre: microscopic view; bottom: ray tracing scheme of light incident in the center and on the sides of the dimple. (Reprinted from [108].)

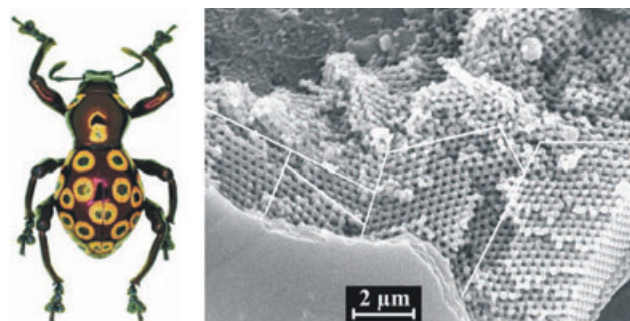


**Figure 24** (online color at: [www.lpr-journal.org](http://www.lpr-journal.org)) Left: weevil *Pachyrrhynchus congestus pavonius*; right: polycrystalline grains of inverse opal occurring in the scales of the weevil (adapted from [120]).

liquid crystals. Their optical properties depend primarily on the pitch of their helicoidal architecture. These types of beetle cuticles most frequently reflect left-handed circularly polarized light, while right-handed circularly polarized light is transmitted [122]. This means that a maximum of 50% of the natural unpolarized light can be reflected. The color selection rule is Bragg's law, and so in this respect the Bouligand structure behaves like a 1D photonic nanoarchitecture with the pitch value taken as the period. Light is selectively reflected when the wavelength  $\lambda_0$  matches the pitch  $p$  of the helix, such that  $\lambda_0 = np \cos \theta$ , where  $n$  is the effective refractive index and  $\theta$  is the angle between the light propagation direction and the helix axis. This type of structure frequently occurs in nature [123, 124], but not necessarily for producing optical effects: its mechanical resistance is also exceptional. A very detailed investigation of polarization and color effects in the light reflected from the cuticle of *Chrysophora chrysochlora*, *Plusiotis resplendens*, and *Cetonischema jousselini* was recently reported by Hegedüs et al [125]. Circular polarization effects were reported in the case of manuka beetles (*Pyronota festiva*), which may have various colors. The most frequent color is green, but other colors such as purple, blue, orange, red, or brown are also encountered [126]. Surprisingly, the structure revealed by TEM micrographs does not show a Bouligand-type structure, but, instead, a 'dimpled' multilayer [126], as discussed in the case of tiger beetles. The difference lies in the fact that the distance of neighboring dimples is on the micrometer scale, while in the case of tiger beetles this distance is closer to the 10 micrometer scale. The dimples of the manuka beetles are filled by a transparent medium.

### 5.5. Intercalated structures

Naturally occurring structures may be combinations of photonic nanoarchitectures of one, two, or three dimensions, as was already discussed in the case of Lycaenid butterfly scales. The combination may be achieved by interpenetrating the elementary nanoarchitectures in Figs. 6a–c, which we refer to as intercalated nanoarchitectures. An example was reported recently in the hercules beetle, *Dynastes hercules*. The beetle appears khaki-green in a dry atmosphere and turns black passively under high humidity levels [72]. SEM images, spectrophotometric measurements and physical modeling were used to unveil the mechanism of this color switch. The greenish color that is visible in the dry state originates from a widely open porous layer located 3  $\mu\text{m}$  below the cuticle surface. As revealed by SEM, the external wax layer exhibits frequent cracks, which allow for the penetration of water into deeper layers. The structure responsible for the dry color is 3D [72] (Fig. 25b). Unexpectedly, diffraction plays a significant role in the broadband coloration of the cuticle in the dry state. The backscattering caused by the layered structure disappears when water infiltrates the structure and weakens the refractive index contrast. The model structure shown in Fig. 25c can be regarded as the structures in Figs. 6a and b, intercalated into each other. The structure observed in SEM images

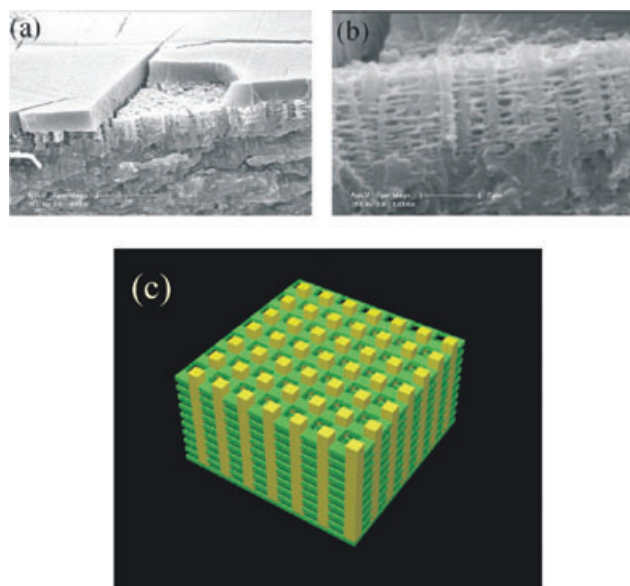


**Figure 25** (online color at: [www.lpr-journal.org](http://www.lpr-journal.org)) SEM micrographs and model structure of the cuticle of the *Dynastes hercules* beetle. a) There is an external wax layer with a number of cracks that allow water to penetrate into the structure. b) Image used to obtain the parameter of the structure for the modeling. c) Intercalated model structure. (Reproduced from [72].)

is more complex and disordered than a simple multilayer. The coloring layer is an array of strong vertical columns, perpendicular to the cuticle surface, which supports a layered network of horizontal filaments, forming thin permeable plates. The separation between the vertical columns is not much larger than the separation between the horizontal filamentary layers, so that this criss-crossed structure should be classified as a 3D PhC, when disorder is disregarded. Further evidence that this structure is at the origin of the color change is provided by the fact that a strong mechanical stress applied on the elytra causes the green region to become black. This suggests that the stress drastically reduces the layer spacing, creating an almost continuous medium and effectively destroying the reflector without any wetting. Detailed, full 3D calculations of the structure in the dry and wet states were carried out on the basis of the model in Fig. 25c and fully reproduced the experimentally observed visual effects [72].

## 6. Bioinspired and biomimetic applications

### 6.1. Artificial, bioinspired structures

As emphasized above, the naturally evolved photonic nanoarchitectures may constitute a valuable source of inspiration for designing and manufacturing new types of artificial photonic nanoarchitectures with various applications.

The unusual multilayer structure of *Chrysochroa vittata* [27] has been successfully reproduced. As shown in

Fig. 17, the artificial structure generates the visual effect seen on the insect. Only the principle of construction of the multilayer (for details, see Section 5.1) was extracted from the biological structure; very different materials were used to realize its artificial counterpart. The chitin plate (refractive index of 1.56) was replaced by a layer of silicon oxide (SiO; refractive index of 1.9). To maintain the dominant wavelength reflected by the structure, a reduction of the multilayer period to 180 nm was required, with the SiO layers 170 nm thick. The periodically repeated air layer with spacers was considered much too complicated, as it would require separate production of every period slab, with one surface appropriately etched to define the spacers. The purpose of this irregular interlayer is simply to produce a periodic perturbation and open the 1D photonic gaps. The location (primarily, the spacing) of these perturbing planes is crucial to define the location of the spectral gap, but the exact nature of the perturbation is not essential, as long as it does not change the average refractive index in a very significant way. The process was simplified by replacing the roughly planar air gaps of the insect's structure by a very thin layer of metal occupying the same positions. This perturbation defined the required periodic dielectric response, adequately contrasting with the SiO response. Nickel was chosen as the metal spacer, in the form of thin layers approximately 10 nm thick. As shown in Fig. 17, the bioinspired approach was completely successful in reproducing the desired visual effects. A detailed analysis of the possibilities offered by such a bioinspired approach was conducted by Deparis et al [101, 127]. They designed and fabricated periodic TiO<sub>2</sub>/SiO<sub>2</sub> multilayer films in order to demonstrate the concept of structurally tuned iridescent surfaces [101]. Two structures were designed in which the period and the TiO<sub>2</sub>/SiO<sub>2</sub> layer thickness ratio were varied in such ways that the films displayed radically different iridescent aspects: one had a reddish-to-greenish changing hue (*Chrysochroa vittata* [27]) while the other had a stable bluish hue (*Hoplia coerulea* [99]). In comparison to the *Chrysochroa*'s design, the *Hoplia*'s design involves a lower index contrast and a more balanced distribution between the thicknesses of high- and low-index layers. The design of the films was carried out following an original theoretical approach for predicting the dominant reflected wavelength of periodically layered materials [127]. The concept of spectral richness was introduced, which is defined as the spectral shift of the dominant reflected wavelength as the angle is increased from normal to grazing incidence:  $\delta\lambda_\theta = \lambda_{\theta=0} - \lambda_\theta$ . The iridescence of the 1D PhC was expressed in terms of the dominant reflected wavelength ( $\lambda_{\theta=0}$ ) and the spectral richness ( $\delta\lambda_\theta$ ). Calculated maps of these quantities were used to precisely tune the parameters of the artificial structures to reproduce the behavior of the biological blueprints. The fabricated samples were characterized by specular reflectance/transmittance measurements, and it was found that they reproduced the behavior of the biological models with high fidelity.

The quasiordered, perforated layer-type nanoarchitectures found in the scales of Lycaenid butterflies (see Section 5.2) were reproduced by the deposition of well-separated indium (In) nanoparticles with near-spherical shape and

diameters close to 50 nm on SiO. The mixed SiO–In layers were separated by pure SiO layers [26]. This choice was motivated by the possibility of oxidizing In under relatively mild conditions, while the SiO layer is unaffected at such conditions (in air at 300 °C). In<sub>2</sub>O<sub>3</sub> has a refractive index of  $n = 1.9$ , close to that of SiO, so that the oxidation can be regarded as a procedure to tailor the size of In particles, without inducing major modifications in the other optical components of the system. Initially, five consecutive layer pairs (SiO/SiO–In) were deposited, and the sample was characterized by normal-incidence reflectance measurements. Then, the In nanoparticles were partially converted to In<sub>2</sub>O<sub>3</sub> via controlled oxidation. The conversion process was monitored by X-ray diffraction. The experiment aimed to model the behavior of the scales of *Albulina metallica* (Figs. 21e–j). The reflectance measurement was repeated after the oxidation treatment, and it was found that the spectral maximum was shifted towards shorter wavelengths by approximately 100 nm, in accordance with model calculations based on the Maxwell-Garnett theory. The experimental data confirmed that, indeed, the size and distance of the perforations, distributed in a quasicrystalline way in the Lycaenid scales, can determine the wavelength of the scattered light. Similar composites may lead to inexpensive ways of producing bioinspired coatings with tunable properties.

Another field in which bioinspired photonic nanoarchitectures may find application is in the increasingly complex technologies used to prevent counterfeiting. For example, the polarization effects found in the curved scales of the male *Suneve coronata* butterfly may be of use in protecting banknotes against counterfeiting [29]. As revealed by SEM micrographs, the cover scales of these butterflies have a cross section similar to those of the dorsal (blue) side of *Cyanophrys remus* (Fig. 11). As opposed to the very flat scales of *C. remus*, the scales of *S. coronata* have a strong curvature. It is this curvature that is the cause of the special polarization effects that appear under TM and TE polarization conditions. The TM conditions are realized when the electric field oscillates normal to the ridges of the scale, while the TE conditions are achieved when the electric field oscillates parallel with the ridges [29]. Berthier et al. showed that, by using a properly structured multilayer, color changes of patterns can be achieved, which may be applied in the field of anti-counterfeiting [29].

## 6.2. Nanoimprint lithography

Nanoimprint lithography [128] is an increasingly popular method for generating complex 3D patterns on the nanoscale. Recently, this technique was used to produce a photonic waveguide in silicon [129]. Frequently, the bottleneck is the manufacturing of the master stamp [130], which can then be replicated at low cost using nanoimprint lithography. Butterfly scales serve as a naturally occurring mold for producing nanoscale features and have been used by several groups to reproduce the nanoarchitectures occurring in scales.

Ordered lead lanthanum zirconate titanate (PLZT) structures with micrometer and submicrometer periods were created by an impression-based sol-gel process, in which PLZT was used as the ceramic precursor and various butterfly wings were used as biological templates [131]. The butterfly wing templates were impressed on the wet PLZT sol layer fabricated by the spin-coating method, and liquid PLZT sol was used to fill the interstices of the butterfly wing templates through capillary action. Finally, the wing templates were removed by calcination. This is an example of a simple, inexpensive, and photo- and electron beam lithography-free method for the fabrication of 2D ordered microstructures using natural biological templates. The nanostructures produced can be used to study the effect of periodic submicrometer dimension and PBG properties of functional ceramics [131].

Although it is not exactly related to the reproduction of color-generating biological nanoarchitectures, the successful use of cicada wings as bio-stamps [130] is worth mentioning here. In this case, a biological template was again successfully transferred to various substrates. Using these natural stamps, nanowell arrays (negative structures of cicada wings) have been fabricated on a polymer support. Furthermore, the nanowell arrays can be transferred to a silicon substrate by reactive ion etching, thus achieving an antireflective property. Using patterned poly(methyl methacrylate) as a mold, hexagonal gold-pillar arrays similar to the surface of cicada wings can also be obtained via thermodeposition [130]. In another replication experiment that also used cicada wings, substrates for surface-enhanced Raman scattering (SERS) were prepared by depositing gold or silver on the wings [132]. The dimensions of the pillars are comparable to the roughness scale of SERS substrates. SERS measurements performed on silver- and gold-coated wings displayed enhancement factors of approximately 10<sup>6</sup>, with no apparent background contribution from the wing [132].

Nanocasts consisting of red-light-emitting cubic Y<sub>2</sub>O<sub>3</sub>:Eu phosphors were made from butterfly wing scale biotemplates [133]. The casts faithfully reproduced the fine submicrometer-size detail of the scales, as evidenced by both SEM and cathodoluminescent images collected from the same sample areas. Precursor Y<sub>2</sub>O<sub>3</sub>:Eu<sup>3+</sup> phosphor solutions were used to prepare filled and inverse butterfly Y<sub>2</sub>O<sub>3</sub>:Eu<sup>3+</sup> phosphor structures. A whole butterfly wing (approximately 2 cm by 3 cm) was placed between two quartz plates containing a film of precursor Y<sub>2</sub>O<sub>3</sub>:Eu<sup>3+</sup> phosphor solution, and the slides were then pressed together and dried. When the precursor solution became opaque, it was placed in a furnace and gradually heated to 700 °C, removing the original scale by calcination. Cathodoluminescent images and high-resolution SEM images were collected from the same area of the nanocasts, revealing valuable information regarding the nature of the internal structure of the casts [133].

Butterfly scales were used to generate more efficient light-harvesting surfaces for dye-sensitized solar cells, or Grätzel cells [30]. Various novel photoanode structures with potential application in dye-sensitized solar cells were produced using butterfly wings as biotemplates. Quasi-

honeycomb-like structures, shallow concavity structures, and cross-ribbing structures were made out of fluorine-doped tin oxide-coated glass, using the scales of *Papilio paris* and *Thaumantis diores*. The butterfly wings were pre-treated in advance to remove salts and proteins. The pre-treated butterfly wings were then immersed in a titanium sulfate precursor solution, maintained at constant temperature over 60 °C for 24 h or more. On removal from the precursor solution, the wings were rinsed thoroughly with alcohol, placed on the layer of the colloidal TiO<sub>2</sub> and covered by piece of glass. The specimen was then placed into an oven, and the temperature was ramped up to 500 °C using a slow heating rate of 1 °C/min in air and kept at that temperature for 2 h. This resulted in the complete removal of the chitinous material. The morphologies of the photoanodes, which were patterned from the original butterfly wings, exhibited a higher light-harvesting efficiency than a normal titania photoanode without biotemplates due to the special nano- and microstructures. It is proposed that this can lead to an improvement in overall solar cell efficiency [30]. This finding may be related to the observation that the structural black of *Papilio ulyssees joreia* is a deeper black than pigmental blacks because of the specialized nanoarchitectures [134], which capture light with a very high efficiency.

### 6.3. Organic/inorganic composites built on natural nanoarchitectures

Another way of using biotemplates is to coat biological nanoarchitectures using different methods of thin-film deposition. After deposition, the organic template may or may not be removed. For example, the scales of the *Morpho peleides* butterfly were covered with conformal, thin layers of Al<sub>2</sub>O<sub>3</sub> using atomic layer deposition (ALD) [135]. In ALD, the precursor materials are introduced sequentially. The first material is introduced and allowed to adsorb on the surface, and then the excess material is evacuated. Following that evacuation, the second precursor is introduced and allowed to react with the first, and this process is repeated cyclically. The two precursors used for Al<sub>2</sub>O<sub>3</sub> deposition were Al(CH<sub>3</sub>)<sub>3</sub> and deionized water. During the replication, the thickness of the Al<sub>2</sub>O<sub>3</sub> layer can be controlled very accurately by varying the number of deposition cycles. The growth rate was 1 Å per cycle at a reaction temperature of 100 °C [135]. It was shown by optical microscopy that with an increase in alumina layer thickness, the original blue color of the scales shifts through green (10 nm), yellow (20 nm), pink (30 nm), and violet (40 nm). After applying the Al<sub>2</sub>O<sub>3</sub> layer, the original butterfly template can then be completely removed by annealing the sample at 800 °C for 3 h in ambient atmosphere. Examination with TEM revealed perfect replication: the calcinated alumina replicas showed the same reflectance maximum as the original wing [135].

Recently, low-temperature ALD at 100 °C was used to reproduce the nanoarchitectures in the scales of the *Papilio blumei* butterfly with TiO<sub>2</sub> [136]. Depending on the structural integrity of an initially sealed scale, it was possible not only to replicate the outer, but also the inner and more

complex surfaces of the structure, each resulting in distinct multicolor optical behavior as revealed by experimental and theoretical data. The *P. blumei* scale has a closed structure, so that on a complete scale, the TiO<sub>2</sub> layer will be deposited only in the exterior. As a consequence, the optical behavior in the long-wavelength side of the visible is continuously shifted with the increase of the layer thickness from 10 to 50 nm, but the position of the original reflectance maximum is maintained [136]. When the TiO<sub>2</sub> was deposited in the interior of a cracked scale, a shift of the original reflectance maximum was also observed.

Another conformal coating method, which can be used to convert organic templates unable to withstand high temperatures or corrosive chemical processes into more resistant mineralized structures, is conformal evaporated film-by-rotation (CEFR). The CEFR technique has recently been devised to fabricate accurate replicas of different biotemplates, with features on the microscale and nanoscale distributed over a curved surface [137]. The CEFR technique is particularly well suited for biomimetization, since the temperatures involved are sufficiently low and the replication process occurs in a non-corrosive environment, thereby avoiding damage and distortion of the carbon-, hydrogen-, and oxygen-based organic skeletons. Chalcogenide GeSbSe glasses were used for the replication. These glasses were chosen due to their good optical properties as well as their good mechanical properties. These glasses are characterized by their large values of refractive index, within the visible and infrared ranges. Furthermore, they are of great technological importance because of their high transmittance in the infrared range and the possibility of modifying their optical band gap and refractive index by illumination [137]. The wings of the *Battus philenor* butterfly were successfully reproduced using a commercial chalcogenide glass of nominal composition Ge<sub>28</sub>Sb<sub>12</sub>Ge<sub>60</sub>, depositing an amorphous GeSbSe thin film on the butterfly wing having a typical thickness of 500 nm. SEM and reflectance measurements showed that the original wing and the replica have similar structure and optical behavior.

### 6.4. Direct applications of natural nanoarchitectures

Recently, butterfly wings and wing pieces were successfully applied in a new field: selective chemical sensing [20, 21]. This application is based on the small but measurable alteration of the refractive index of air in the presence of various gases and vapors. Potyrailo et al [20] used the wings of one butterfly species (*Morpho sulkowskyi*) and sophisticated data analysis software to demonstrate selective chemical sensitivity of the reflectance measured on the wings of *M. sulkowskyi*. Using a different approach, Biró et al [21] used several different butterfly wings with a simple experimental setup and white light illumination and demonstrated that different butterflies possessing structural colors give different signals in the presence of organic solvent vapors. They found that the wing of *Chrysiridia rypheus*, an extremely

colorful moth also known as the sunset moth, gives distinct signals for seven different organic solvent vapors. The scales of this butterfly have been investigated in detail by Yoshioka and Kinoshita [138]. The chemical selectivity of the optical response of the butterfly wings possessing structural color offers the possibility to use them in chemically selective detectors. These detectors, when combined with computer-aided data processing, are able to recognize various gases or vapors in a few seconds. The sensing principle was demonstrated using carbon nanotubes with chemical functionalizations that induced a chemically selective response in their electrical resistance, reacting to the composition of the surrounding atmosphere [139]. Using butterfly wings as sensors may have several advantages, including the possibility of optical readout without wiring (for example in explosion risk environments) and the very low cost and environmentally friendly production of the nanostructured sensor element.

### 6.5. Special applications

A few special application possibilities will be briefly addressed in this section. It was shown that, under artificial illumination, the presence of the PBG material in the scales of the *Polyommatus daphnis* butterfly causes the maximum wing temperature to be approximately 5 °C lower than in the case of the *Polyommatus marcidus*, a related species that lives at high altitudes [81] and has no structural colors [140]. This example demonstrates that photonic nanoarchitectures may have a role in thermal management: properly designed, multilayer nanoarchitectures may be able to reflect wide ranges of solar radiation. Moreover, if combined with microfluidics, such as in the tortoise beetle (*Charidotella egregia* [100]), such reflectors could even be switchable.

Another application that may seem unusual is the identification of butterfly species by non-experts. Lepidopterist experts use the often complex patterns on the wings of butterflies to identify species that live syntopically and synchronously, such as blue Lycaenids. On the other hand, it is highly unlikely that the butterflies themselves, with the limited processing capacity of their brains (due to size), use the same recognition mechanism in flight. More likely, their vision allows them to distinguish the different spectral signatures of superficially similar looking species. Spectroscopic measurements confirm that related, but different species have characteristic spectral signatures [141, 142].

## 7. Perspectives

In this review nanoarchitectures utilized in color-generation mechanisms of butterflies and beetles have been presented, e.g. the 'purposeful' use of disorder to achieve certain visual effects and the usefulness of relatively mild refractive index contrast of alternating layers offering large spectral richness to various structures. From these finding new technical applications may arise. Investigations of the structure and optical properties of the white filaments in the bracts of edelweiss

(*Leontopodium nivale*) [143] revealed that this plant protects itself from the harmful UV radiation by nanostructured filaments. The filaments are able to selectively absorb UV radiation, while visible light crosses the nanofilaments with very little loss. Subsequently, a group working in the field of polymer chemistry successfully reproduced the structure of these filaments for UV protection [144]. In addition to already accomplished achievements, also new and very interesting directions may be opened by the recently discovered fluorescence enhancement of the papiliochrome pigment in the ridges of *Troides magellanus* [18]. To date, little is known about new phenomena that may arise in geometrically confined fluorescent structures.

Biomimetic and bioinspired approaches will find increasing applications in many scientific disciplines. The strong convergence of biology, physics, chemistry, and materials science in the range of nanoscale dimensions will very likely affect many of the ways we see and understand the world, and the ways we produce goods. Nature has given us a great repository of photonic nanostructures that wait to be discovered. However, keeping in mind that due to human intervention many species will disappear forever in the coming decades, this should be further impetus to study and understand these living creatures while they are still existent and can be studied in their natural habitats.

**Acknowledgements.** The authors wish to thank Dr. Ing. Olivier Deparis (FUNDP) for critically reading the manuscript and for useful comments. L. P. B. gratefully acknowledges financial support for mobility from the CGRI-TÉT and the FNRS-HAS. Many of the results reviewed within this paper were made possible by financial support within EU6 NEST/PATHFINDER/BioPhot-12915. The work in Hungary benefited from the support of OTKA-NKTH grant 67793. The authors acknowledge the use of the Namur Interuniversity Scientific Computing Facility (Namur-ISCF).

**Received:** 1 March 2009, **Revised:** 4 December 2009,

**Accepted:** 4 December 2009

**Published online:** 18 January 2010

**Key words:** Photonic crystal, photonic band gap, color, nanoarchitectures, butterfly, beetle, scale, elytra, bioinspired, biomimetic.



**László Péter Biró** is the head of the Nanostructures Department in the Research Institute for Technical Physics and Materials Science of the Hungarian Academy of Sciences. He received his Ph.D. degree in 1997 from the Technical University of Budapest after contributing to STM and AFM investigation of surface nanostructures produced by ion irradiation. In 2005, he became a Doctor of the Hungarian Academy of Sciences for his work on carbon nanotube-type nanostructures. Currently, he is interested in photonic nanoarchitectures of biological origin and bioinspiration.



**Jean-Pol Vigneron** is a professor of physics at the University of Namur, Belgium, and a member of the Royal Academy for Sciences, Letters and Arts of Belgium. He received his Ph.D. degree from the University of Liège in 1979. While working at IBM at the Thomas Watson Research Center in Yorktown Heights, he developed computer models for shallow- and deep-level impurities in semiconductors. Back in Belgium, he worked on the interpretation of local-probe images, electron energy loss and optical spectra of solids. Currently, his interest has evolved to the investigation of the physical origin of visual effects developed by living organisms.

## References

- [1] E. Yablonovitch, *Phys. Rev. Lett.* **58**, 2059 (1987).
- [2] S. John, *Phys. Rev. Lett.* **58**, 2486 (1987).
- [3] A. R. Parker, *J. Exp. Biol.* **201**, 2343 (1998).
- [4] M. Srinivasarao, *Chem. Rev.* **99**, 1935 (1999).
- [5] R. Hooke, *Micrographia: Or Some Physiological Descriptions of Minute Bodies made by Magnifying Glasses with Observations and Inquiries thereupon* (1665) (Dover, New York, 1961).
- [6] I. Newton, *Opticks: Or, a Treatise of the Reflections, Refractions, Inflections and Colours of Light* (1704) (Dover, New York, 1952).
- [7] Lord Rayleigh, *Phil. Mag.* **37**, 98 (1919).
- [8] T. Lenau and M. Barfoed, *Adv. Eng. Mater.* **10**, 299 (2008).
- [9] A. R. Parker, *Proc. R. Soc. Lond. B* **265**, 967 (1998).
- [10] D. J. Kemp, *Proc. R. Soc. B* **274**, 1043 (2007).
- [11] D. J. Kemp, *Behav. Ecol.* **19**, 1 (2008).
- [12] A. Loyau, D. Gomez, B. Moureau, M. Théry, N. S. Hart, M. Saint Jalme, A. T. D. Bennett, and G. Sorci, *Behav. Ecol.* **18**, 1123 (2007).
- [13] W. H. Wente and J. B. Phillips, *Am. Naturalist* **162**, 461 (2003).
- [14] S. Merilaita, J. Tuomi, and V. Jormalainen, *Biol. J. Linn. Soc.* **67**, 151 (1999).
- [15] K. Kertész, Zs. Bálint, Z. Vértésy, G. I. Márk, V. Lousse, J. P. Vigneron, M. Rassart, and L. P. Biró, *Phys. Rev. E* **74**, 021922 (2006).
- [16] A. B. Bond and A. C. Kamil, *Nature* **415**, 609 (2002).
- [17] D. G. Ruxton, T. N. Sherratt, and M. P. Speed, *Avoiding Attack: the Evolutionary Ecology of Crypsis, Warning Signals and Mimicry* (Oxford University Press, Oxford, 2004).
- [18] J. P. Vigneron, K. Kertész, Z. Vértésy, M. Rassart, V. Lousse, Zs. Bálint, and L. P. Biró, *Phys. Rev. E* **78**, 021903 (2008).
- [19] J. P. Vigneron, J. M. Pasteels, D. M. Windsor, Z. Vértésy, M. Rassart, T. Seldrum, J. Dumont, O. Deparis, V. Lousse, L. P. Biró, D. Ertz, and V. Welch, *Phys. Rev. E* **76**, 031907 (2007).
- [20] R. A. Potyrailo, H. Ghiradella, A. Vertiatikh, K. Dovidenko, J. R. Cournoyer, and E. Olson, *Nature Photon.* **1**, 123 (2007).
- [21] L. P. Biró, K. Kertész, Z. Vértésy, and Zs. Bálint, *Proc. SPIE* **7057**, 705706 (2008).
- [22] G. Zhang, J. Zhang, G. Xie, Z. Liu, and H. Shao, *Small* **2**, 1440 (2006).
- [23] J. Huang, X. Wang, and Z. L. Wang, *Nano Lett.* **6**, 2325 (2006).
- [24] J. Silver, R. Withnall, T. G. Ireland, G. R. Fern, and S. Zhang, *Nanotechnology* **19**, 095302 (2008).
- [25] S. Zhu, D. Zhang, Z. Li, H. Furukawa, and Z. Chen, *Langmuir* **24**, 6292 (2008).
- [26] K. Kertész, G. Molnár, Z. Vértésy, A. A. Koós, Z. E. Horváth, G. I. Márk, L. Tapasztó, Zs. Bálint, I. Tamáska, O. Deparis, J. P. Vigneron, and L. P. Biró, *Mater. Sci. Eng. B* **149**, 259 (2008).
- [27] J. P. Vigneron, M. Rassart, C. Vandembem, V. Lousse, O. Deparis, L. P. Biró, D. Dedouaire, A. Cornet, and P. DeFrance, *Phys. Rev. E* **73**, 041905 (2006).
- [28] J. Wang, J. Liang, H. Wu, W. Yuan, Y. Wen, Y. Song, and L. Jiang, *Polym. Int.* **57**, 509 (2007).
- [29] S. Berthier, J. Boulenguez, and Z. Bálint, *Appl. Phys. A* **86**, 123 (2007).
- [30] W. Zhang, D. Zhang, T. Fan, J. Gu, J. Ding, H. Wang, Q. Guo, and H. Ogawa, *Chem. Mater.* **21**, 33 (2009).
- [31] A. R. Parker and H. E. Townley, *Nature Nanotechnol.* **2**, 347 (2007).
- [32] A. Saito, Y. Miyamura, Y. Ishikawa, J. Murase, M. Akai-Kasaya, and Y. Kuwahara, *Proc. SPIE* **7205**, 720506 (2009).
- [33] H. F. Nijhout, *The Development and Evolution of Butterfly Wing Patterns* (Smithsonian Institution Press, 1991).
- [34] H. Ghiradella, *J. Morphol.* **150**, 279 (1975).
- [35] H. Ghiradella, *Ann. Entomol. Soc. Am.* **77**, 637 (1984).
- [36] H. Ghiradella, in: *Microscopic Anatomy of Invertebrates*, Vol. 11A, Insecta, edited by F. N. Harrison and M. Locke (Wiley-Liss, New York, 1998), p. 257.
- [37] H. Ghiradella, *J. Morphol.* **202**, 69 (1989).
- [38] H. Ghiradella, *Appl. Opt.* **30**, 3492 (1991).
- [39] S. Kinoshita and S. Yoshioka, *Chem. Phys. Chem.* **6**, 1442 (2005).
- [40] A. E. Seago, P. Brady, J.-P. Vigneron, and T. D. Schultz, *J. R. Soc. Interf.* **6** (Suppl. 2), S165 (2009).
- [41] V. Welch, V. Lousse, O. Deparis, A. Parker, and J. P. Vigneron, *Phys. Rev. E* **75**, 041919 (2007).
- [42] J. F. V. Vincent and U. G. K. Wegst, *Arthropod Struct. Devel.* **33**, 187 (2004).
- [43] P. Vukusic, J. R. Sambles, C. R. Lawrence, and R. J. Wootton, *Proc. R. Soc. Lond. B* **266**, 1403 (1999).
- [44] S. Berthier, *Iridescences: les Couleurs Physiques des Insectes* (Springer, Paris, 2003). English edition: *Iridescences: the Physical Colors of Insects* (Springer, Berlin, 2007).
- [45] B. Gralak, G. Tayeb, and S. Enoch, *Opt. Express* **9**, 567 (2001).
- [46] S. Kinoshita, S. Yoshioka, Y. Fujii, and N. Okamoto, *Forma* **17**, 103 (2002).
- [47] S. Kinoshita, S. Yoshioka, and K. Kawagoe, *Proc. R. Soc. Lond. B* **269**, 1417 (2002).
- [48] S. Berthier, E. Charron, and A. Da Silva, *Opt. Commun.* **228**, 349 (2003).
- [49] L. Plattner, *J. R. Soc. Interf.* **1**, 49 (2004).
- [50] S. Berthier, *Photonique des Morphos (Morpho photonics)* (in press).
- [51] D. J. Kemp, *Trends Ecol. Evol.* **17**, 298 (2002).
- [52] D. G. Stavenga, H. L. Leertouwer, P. Pirih, and M. F. Wehling, *Opt. Express* **17**, 193 (2009).
- [53] C. Lopez, *Adv. Mater.* **15**, 1679 (2003).
- [54] D. J. Norris and Y. A. Vlasov, *Adv. Mater.* **13**, 371 (2001).
- [55] A. Hartsuiker and W. L. Vos, *Langmuir* **24**, 4670 (2008).

- [56] H.-B. Su and S. Kawata, Two-Photon Photopolymerization and 3D Lithographic Microfabrication (Springer, Berlin/Heidelberg, 2004).
- [57] E. R. Dedman, D. N. Sharp, A. J. Turberfield, C. F. Blanford, and R. G. Denning, *Photon. Nanostruct.* **3**, 79 (2005).
- [58] G. M. Gratson, M. Xu, and J. A. Lewis, *Nature* **428**, 386 (2004).
- [59] J. F. V. Vincent, O. A. Bogatyreva, N. R. Bogatyrev, A. Bowyer, and A.-K. Pahl, *J. R. Soc. Interf.* **3**, 471 (2006).
- [60] K. Edagawa, S. Kanoko, and M. Notomi, *Phys. Rev. Lett.* **100**, 013901 (2008).
- [61] L. P. Biró, K. Kertész, Z. Vértésy, G. I. Márk, Zs. Bálint, V. Lousse, and J.-P. Vigneron, *Mater. Sci. Eng. C* **27**, 941 (2007).
- [62] E. Yablonovitch, *J. Opt. Soc. Am. B* **10**, 283 (1993).
- [63] E. Yablonovitch, *Opt. Photonics News* **18**, 12 (2007).
- [64] Lord Rayleigh, *Phil. Mag.* **24**, 145 (1887).
- [65] F. Abelès, *Ann. Phys. (France)* **12**, 504 (1948).
- [66] P. Yeh, A. Yariv, and C. S. Hong, *J. Opt. Soc. Am.* **67**, 423 (1977).
- [67] K. M. Ho, C. T. Chan, and C. M. Soukoulis, *Phys. Rev. Lett.* **65**, 3152 (1990).
- [68] E. Yablonovitch, T. J. Mitter, and K. M. Leung, *Phys. Rev. Lett.* **67**, 2295 (1991).
- [69] E. Yablonovitch and T. J. Gmitter, *Phys. Rev. Lett.* **63**, 1950 (1989).
- [70] J. P. Vigneron and V. Lousse, *Proc. SPIE* **6128**, 61281G (2006).
- [71] V. L. Welch, J. P. Vigneron, and A. R. Parker, *Curr. Biol.* **15**, R985 (2005).
- [72] M. Rassart, J.-F. Colomer, T. Tabarrant, and J. P. Vigneron, *New J. Phys.* **10**, 033014 (2008).
- [73] H. S. Sözüer, J. W. Haus, and R. Inguva, *Phys. Rev. B* **45**, 13962 (1992).
- [74] Z. Bai, J. Demmel, J. Dongarra, A. Ruhe, and H. Van Der Vorst, eds., *Templates for the Solution of Algebraic Eigenvalue Problems: A Practical Guide* (SIAM, Philadelphia, PA, 2000).
- [75] P. Vukusic and I. Hooper, *Science* **310**, 1151 (2005).
- [76] A. Taflove and S. C. Hagness, *Computational Electrodynamics: The Finite-Difference Time-Domain Method*, 3rd edn. (Artech House, Boston, MA, 2005).
- [77] J. P. Berenger, *J. Comput. Phys.* **114**, 185 (1994).
- [78] R. T. Lee and G. S. Smith, in: *Proceedings of the 2007 IEEE Antennas and Propagation Society International Symposium, Honolulu, HI (IEEE, 2008)*, pp. 4352–4355.
- [79] J. B. Pendry, *Low Energy Electron Diffraction* (Academic Press, London, 1974).
- [80] P. M. Bell and J. B. Pendry, L. Martín-Moreno, and A. J. Ward, *Comput. Phys. Commun.* **85**, 306 (1995).
- [81] L. P. Biró, Zs. Bálint, K. Kertész, Z. Vértésy, G. I. Márk, Z. E. Horváth, J. Balázs, D. Méhn, I. Kiricsi, V. Lousse, and J.-P. Vigneron, *Phys. Rev. E* **67**, 021907 (2003).
- [82] J. P. Vigneron, V. M. Lousse, L. P. Biró, Z. Vértésy, and Zs. Bálint, *Proc. SPIE* **5733**, 308 (2005).
- [83] P. Debye, *Ann. Phys.* **348**, 49 (1913).
- [84] S. Preble, M. Lipson, and H. Lipson, *Appl. Phys. Lett.* **86**, 061111 (2005).
- [85] A. Gondarenko, S. Preble, J. Robinson, L. Chen, H. Lipson, and M. Lipson, *Phys. Rev. Lett.* **96**, 143904 (2006).
- [86] A. Argyros, S. Manos, M. C. J. Large, and D. R. McKenzie, G. C. Cox, and D. M. Dwarde, *Micron* **33**, 483 (2002).
- [87] L. P. Biró, Zs. Bálint, Z. Vértésy, K. Kertész, G. I. Márk, V. Lousse, and J.-P. Vigneron, *Nanopages* **1**, 195 (2006).
- [88] R. O. Prum, T. Quinn, and R. H. Torres, *J. Exp. Biol.* **209**, 748 (2006).
- [89] R. O. Prum and R. Torres, *J. Exp. Biol.* **206**, 2409 (2003).
- [90] R. O. Prum and R. H. Torres, *J. Exp. Biol.* **207**, 2157 (2004).
- [91] D. G. Stavenga, M. A. Giraldo, and B. J. Hoenders, *Opt. Express* **14**, 4880 (2006).
- [92] S. Yoshioka and S. Kinoshita, *Proc. R. Soc. Lond. B* **271**, 581 (2004).
- [93] Ch. Lawrence, P. Vukusic, and R. Sambles, *Appl. Opt.* **41**, 437 (2002).
- [94] J. A. Noyes, P. Vukusic, and I. R. Hooper, *Opt Express* **15**, 4351 (2007).
- [95] J. Boulenguez, S. Berthier, and J. P. Vigneron, *Physica B* **394**, 217 (2007).
- [96] K. Kertész, Zs. Bálint, Z. Vértésy, G. I. Márk, V. Lousse, J.-P. Vigneron, and L. P. Biró, *Curr. Appl. Phys.* **6**, 252 (2006).
- [97] A. R. Parker, D. R. McKenzie, and M. C. J. Large, *J. Exp. Biol.* **201**, 1307 (1998).
- [98] T. Hariyama, Y. Takaku, M. Hironaka, H. Horiguchi, Y. Komiya, and M. Kurachi, *Forma* **17**, 123 (2002).
- [99] J. P. Vigneron, J.-F. Colomer, N. Vigneron, and V. Lousse, *Phys. Rev. E* **72**, 061904 (2005).
- [100] J. P. Vigneron, J. M. Pasteels, D. M. Windsor, Z. Vértésy, M. Rassart, Th. Seldrum, J. Dumont, O. Deparis, V. Lousse, L. P. Biró, D. Ertz, and V. Welch, *Phys. Rev. E* **76**, 031907 (2007).
- [101] O. Deparis, M. Rassart, C. Vandembem, V. Welch, J. P. Vigneron, and S. Lucas, *New J. Phys.* **10**, 013032 (2008).
- [102] A. Yoshida, *Forma* **17**, 75 (2002).
- [103] P. Vukusic, J. R. Sambles, C. R. Lawrence, and R. J. Wootton, *Proc. R. Soc. Lond. B* **269**, 7 (2002).
- [104] Ch. Lawrence, P. Vukusic, and R. Sambles, *Appl. Opt.* **41**, 437 (2002).
- [105] A. L. Ingram, V. Lousse, A. R. Parker, and J. P. Vigneron, *J. R. Soc. Interf.* **5**, 1387 (2008).
- [106] T. D. Schultz and M. A. Rankin, *J. Exp. Biol.* **117**, 87 (1985).
- [107] F. Liu, H. Yin, B. Dong, Y. Qing, L. Zhao, S. Meyer, X. Liu, J. Zi, and B. Chen, *Phys. Rev. E* **77**, 012901 (2008).
- [108] J. P. Vigneron, M. Ouedraogo, J.-F. Colomer, and M. Rassart, *Phys. Rev. E* **79**, 021907 (2009).
- [109] S. Berthier, J. Boulenguez, and Z. Bálint, *Appl. Phys. A* **86**, 123 (2007).
- [110] B. D. Wilts, H. L. Leertouwer, and D. G. Stavenga, *J. R. Soc. Interf.* **6** (Suppl. 2), S185 (2009).
- [111] Z. Vértésy, Zs. Bálint, K. Kertész, J. P. Vigneron, V. Lousse, and L. P. Biró, *J. Microsc.* **224**, 108 (2006).
- [112] P. Vukusic, R. Sambles, Ch. Lawrence, and G. Wakely, *Appl. Opt.* **40**, 1116 (2001).
- [113] P. Vukusic, J. R. Sambles, and C. R. Lawrence, *Nature* **404**, 457 (2000).
- [114] P. Vukusic and J. R. Sambles, *Nature* **424**, 852 (2003).
- [115] A. L. Ingram and A. R. Parker, *Phil. Trans. R. Soc. B* **363**, 2465 (2008).
- [116] K. Michielsen and D. G. Stavenga, *J. R. Soc. Interf.* **5**, 85 (2008).
- [117] D. Gaillot, T. Yamashita, and C. J. Summers, *Phys. Rev. B* **72**, 205109 (2005).
- [118] A. R. Parker, V. L. Welch, D. Driver, and N. Martini, *Nature* **426**, 786 (2003).

- [119] V. L. Welch and J.-P. Vigneron, *Opt. Quantum Electron.* **39**, 295 (2007).
- [120] V. Welch, V. Lousse, O. Deparis, A. Parker, and J. P. Vigneron, *Phys. Rev. E* **75**, 041919 (2007).
- [121] J. W. Galusha, L. R. Richey, J. S. Gardner, J. N. Cha, and M. H. Bartl, *Phys. Rev. E* **77**, 050904(R) (2008).
- [122] A. C. Neville and S. Caveney, *Biol. Rev.* **44**, 531 (1969).
- [123] M.-M. Giraud-Guille, *Curr. Opin. Solid State Mater. Sci.* **3**, 221 (1998).
- [124] M. Mitov and N. Dessaud, *Nature Mater.* **5**, 361 (2006).
- [125] R. Hegedüs, G. Szél, and G. Horváth, *Vision Res.* **46**, 2786 (2006).
- [126] L. De Silva, I. Hodgkinson, P. Murray, Q. H. Wu, M. Arnold, J. Leader, and A. McNaughton, *Electromagnetics* **25**, 391 (2005).
- [127] O. Deparis, C. Vandembem, M. Rassart, V. L. Welch, and J.-P. Vigneron, *Opt. Express* **14**, 3547 (2006).
- [128] L. J. Guo, *Adv. Mater.* **19**, 495 (2007).
- [129] Ch. M. Bruinink, M. Burrese, M. J. de Boer, F. B. Segerink, H. V. Jansen, E. Berenschot, D. N. Reinhoudt, J. Huskens, and L. Kuipers, *Nano Lett.* **9**, 2872 (2008).
- [130] G. Zhang, J. Zhang, G. Xie, Z. Liu, and H. Shao, *Small* **2**, 1440 (2006).
- [131] B. Li, J. Zhou, R. Zong, M. Fu, Y. Bai, L. Li, and Q. Li, *J. Am. Ceram. Soc.* **89**, 2298 (2006).
- [132] P. R. Stoddart, P. J. Cadusch, T. M. Boyce, R. M. Erasmus, and J. D. Comins, *Nanotechnology* **17**, 680 (2006).
- [133] J. Silver, R. Withnall, T. G. Ireland, G. R. Fern, and S. Zhang, *Nanotechnology* **19**, 095302 (2008).
- [134] P. Vukusic, J. R. Sambles, and C. R. Lawrence, *Proc. R. Soc. Lond. B* **271** (Suppl.), S237 (2004).
- [135] J. Huang, X. Wang, and Z. L. Wang, *Nano Lett.* **6**, 2325 (2006).
- [136] D. P. Gaillot, O. Deparis, V. Welch, B. K. Wagner, J. P. Vigneron, and Ch. J. Summers, *Phys. Rev. E* **78**, 031922 (2008).
- [137] R. J. Martín-Palma, C. G. Pantano, and A. Lakhtakia, *Appl. Phys. Lett.* **93**, 083901 (2008).
- [138] S. Yoshioka and S. Kinoshita, *Opt. Express* **15**, 2691 (2007).
- [139] Z. E. Horváth, A. A. Koós, K. Kertész, G. Molnár, G. Vértesy, M. C. Bein, T. Frigyes, Z. Mészáros, J. Gyulai, and L. P. Biró, *Appl. Phys. A* **93**, 495 (2008).
- [140] Zs. Bálint and K. Johnson, *Neue Entomol. Nachr. (Marktleuthen)* **68**, 4 (1997).
- [141] Zs. Bálint, P. Boyer, K. Kertész, and L. P. Biró, *J. Nat. Hist.* **42**, 1793 (2008).
- [142] Zs. Bálint, A. Moser, K. Kertész, L. P. Biró, and A. R. Parker, *Ann. Hist.-Natur. Mus. Nat. Hung.* **101**, 63 (2009).
- [143] J. P. Vigneron, M. Rassart, Z. Vértesy, K. Kertész, M. Sarrazin, L. P. Biró, D. Ertz, and V. Lousse, *Phys. Rev. E* **71**, 011906 (2005).
- [144] J. Wang, J. Liang, H. Wu, W. Yuan, Y. Wen, Y. Song, and L. Jiang, *Polym. Int.* **57**, 509 (2007).